Fragmentation through cell-cell adhesion maintains senescent cell viability but promotes debris deposition

Matej Durik[1,2,3,4,9], Daniel Sampaio Gonçalves[1,2,3,4], Tania Knauer-Meyer[1,2,3,4], Coralie Spiegelhalter[1,2,3,4], Nadia Messaddeq[1,2,3,4], Marco Seehawer[5,6,7], Dmitry Bulavin[8], Lars Zender[5,6,7] and William M. Keyes[1,2,3,4,9,]

[1]Institut de Génétique et de Biologie Moléculaire et Cellulaire (IGBMC), Équipe Labellisée Ligue Contre le Cancer, Illkirch, France
[2]UMR7104, Centre National de la Recherche Scientifique (CNRS), Illkirch, France
[3]U1258, Institut National de la Santé et de la Recherche Médicale (INSERM), Illkirch, France
[4]Université de Strasbourg, Illkirch, France
[5]Department of Internal Medicine VIII, University Hospital Tübingen, 72076 Tübingen, Germany
[6]Department of Physiology I, Institute of Physiology, Eberhard Karls University Tübingen, 72076 Tübingen, Germany
[7]Translational Gastrointestinal Oncology Group, German Consortium for Translational Cancer Research (DKTK), German Cancer Research Center (DKFZ), Heidelberg 69120, Germany
[8]Institute for Research on Cancer and Aging of Nice (IRCAN), Université Côte d'Azur, INSERM, CNRS, Nice, France

Keywords: senescence, mitochondria, cell-cell adhesion, debris, aging, cancer, DAMPs,

[9]Correspondence to

Bill Keyes,
IGBMC,
1 Rue Laurent Fries, BP 10142,
67404 Illkirch - CU Strasbourg
France

e-mail: keyesb@igbmc.fr

Matej Durik,
IGBMC,
1 Rue Laurent Fries, BP 10142,
67404 Illkirch - CU Strasbourg
France

e-mail : durikm@igbmc.fr

ABSTRACT

Cellular senescence is a state of stable arrest and secretion linked to aging and disease. Here we identify that senescent cells dispose of large fragments of themselves through cell-to-cell adhesion, which we term senescent-cell adhesion fragments (SCAFs). Found across all senescent types examined, SCAFs lack nuclear material but contain organelles, including damaged mitochondria. Disrupting adherens junctions decreased SCAF formation but induced senescent-cell death, which was caused by an inability to shed damaged mitochondria. Dynamic analyses show that SCAFs ultimately rupture, releasing a complex proteome including damage-associated molecular patterns (DAMPs) and proteins linked to neurodegenerative disease. Functionally, SCAFs activate wound-healing and cancer-related programs, promoting migration and invasion. Altogether, these findings identify a new feature that facilitates senescent cell survival, but the consequence of which is external deposition of damaged intracellular contents, with implications for cancer and aging.

INTRODUCTION

Cellular senescence is a highly dynamic and complex cellular response that can affect all stages of life.[1,2] Senescence is triggered in response to replicative exhaustion, oncogene activation, chemotherapy and various cellular stresses, but it can also be induced in a controlled manner in the context of regeneration or embryonic development.[2–5] Two main characteristics of senescent cells are an irreversible proliferative arrest and a highly active secretory profile called the senescence-associated secretory phenotype (SASP).[4,6] The SASP consists of many signaling molecules such as chemokines, growth factors and extracellular matrix remodelers, and promotes the recruitment of immune cells to remove senescent cells.[7–9]

The outcome of senescence induction can either be beneficial or detrimental, depending on timing and context. Senescent cells play physiological roles during embryonic development, wound healing and regeneration, where they appear transiently, and through the SASP, contribute to tissue patterning, regeneration, growth and repair.[2,10–12] However, it is thought that this process becomes misregulated during aging, with the aberrant accumulation of senescent cells actively contributing to tissue aging.[13,14] In addition, many age-related diseases have an increased senescent cell burden, ranging from idiopathic pulmonary fibrosis (IPF) and arthritis, to Alzheimer's disease (AD), Amyotrophic Lateral Sclerosis (ALS) and Parkinson's disease.[3,15–17] Senescent cells also significantly impact cancer formation, promoting tumor cell proliferation, recurrence after treatment and metastasis.[5,18] Despite frequently containing significant macromolecular damage, including damaged organelles, senescent cells remain alive, and are even resistant to cell death. During recent years, numerous studies have

identified how the elimination or removal of senescent cells in aged or diseased states can be beneficial.[13–15,19,20] Therefore, aberrant induction of senescence is detrimental, and interfering with it can have a beneficial impact on aging and age-related diseases.

However, exactly how cellular senescence contributes to aging or pathology remains unresolved. There is a critical need to better understand the cellular mechanisms of senescence, how these cells persist despite substantial damage, and how they contribute to aging and disease. Here, we unexpectedly find that senescent cells dispose of large fragments of themselves through cell–cell adhesion. We show that this fragmentation is required for senescent-cell survival, yet ultimately results in the rupture of these fragments and the release of diverse intracellular cargo onto neighboring cells and into the extracellular space. We propose that senescent fragments represent another critical step towards our understanding of the link with senescent cells and aging and disease processes.

RESULTS

Senescent cells deposit large fragments through cell-cell adhesion

Cellular senescence is a complex process, with typical markers, including senescence-associated beta-galactosidase (SA-β-gal) activity, and p21 and p16 expression appearing dynamically after induction (Extended data Fig. 1). Our interest was to study the dynamic process of senescence onset and maintenance. To achieve this, we established an *in vitro* model system that would enable us to image and track individual cells becoming senescent over time (Fig. 1A). This involved infecting human IMR-90 fibroblasts with a constitutive GFP-expressing retroviral vector (MSCV-PIG), so that after drug selection, these cells would stably express GFP. Using these GFP-positive fibroblasts, we then either induced senescence by irradiating with 10Gy X-ray irradiation, or left the cells proliferating as controls. Next, either proliferating or irradiated GFP-positive cells were diluted at a ratio of 1:1000 into either proliferating or senescing cells that were negative for GFP (NEG) to achieve the following combinations: proliferating-GFP into proliferating-NEG; senescing-GFP into proliferating-NEG; senescing-GFP into senescing-NEG (Fig. 1A). We reasoned that in such a scenario, the proliferating-proliferating (Prol-Prol) conditions would resemble normal healthy conditions, the senescing into proliferating (Sen-Prol) would resemble low levels of senescence induction, while the senescing into senescing (Sen-Sen) would more closely resemble standard senescent culture conditions, or chronic senescent buildup as seen in damaged and aged tissue.

Following irradiation and plating the various conditions, we imaged the cells each day. Unexpectedly, by 3-5 days post-irradiation, we repeatedly observed small GFP positive

fragments in the cultures of cells induced to senesce, in both the proliferating and senescing environments (Fig. 1B). These were not visible, or were only present at very low levels in the proliferating control conditions. However, when we imaged these fragments at higher resolution, it was clear they were not pieces of cell debris in the media, but were GFP-positive cellular fragments bound to the membranes of adjacent cells (Fig. 1C). To determine the origin of these fragments, we next performed time-lapse imaging of the different culture conditions. In all conditions, cells routinely made contact with neighboring cells in a dynamic manner. In control cells (Prol-Prol), these contacts were non-permanent. Somewhat surprisingly, senescing cells also exhibited quite dynamic behavior, moving around the dish and making contacts. However, in cells induced to become senescent, sometimes these contacts persisted and the cells remained attached as the cells moved apart (Fig. 1D and Supplemental Movie 1). This movement resulted in the generation of long GFP-positive threads pulled between two cells, undergoing stretching and tension. Then, at one point, the senescent cells tore, leaving large GFP-positive fragments attached to the neighboring cell (Fig. 1D). Surprisingly however, following this process, both the fragments and the senescent cells remained intact, suggesting there are initial active membrane repair mechanisms present, even if the fragment may further disintegrate into smaller pieces over time. It appears that the strength of adhesion is quite high, as in some cases, there was clear recoil of the senescent cell following generation of the fragment. This process of adhesion-mediated fragmentation was consistently observed. We quantified the number of fragments at early timepoints, and found these became detectable around 3 days following irradiation, increasing to approx. 10-12 fragments per senescent cell at day 5 (Fig. 1E). This process of fragmentation continued, and similar numbers of fragments were seen at later stages in fully senescent cells (Fig. 1E). Together, this demonstrates that fragmentation is an ongoing and active process associated with senescent cells.

Next, we used image-analysis to quantify the fragment sizes. As these are dynamically-forming structures, there was great variation in the major-axis length, with some fragments stretching along the neighboring cell, while others had already rounded to a smaller size or disintegrated (Fig. 1F). Overall, omitting structures smaller than 2um, which may include secondary disintegration, this demonstrated that fragments are large structures with a mean length of the major axis of 7-8μm (Fig. 1G).

To investigate if cell-cell adhesion is required for this process, we next plated GFP-positive senescing cells at low density, in the absence of neighboring cells. These cells displayed similar senescent features as the previous conditions, but did not generate fragments (Fig. 1H). Together, this uncovers that senescent cells generate large cell fragments through a

111 process of cell-cell adhesion. As a result, we chose to call these “senescent-cell adhesion
112 fragments” (SCAFs).
113
114 As such cellular fragments had not previously been associated with senescent cells, we asked
115 if they were unique to irradiation-induced senescence (IIS) in IMR-90 primary human
116 fibroblasts. To address this we examined other conditions, including oncogene-induced
117 senescence (OIS) in primary fibroblasts, or IIS or chemotherapy-induced senescence (TIS) in
118 human liver cancer cells (Fig. 1I). In each case, SCAFs were detectable attached to
119 neighboring cells. Similar fragments were also detected in mouse primary dermal fibroblasts
120 (shown later in Extended data Fig. 6). Therefore, in every situation examined, senescent cells
121 were found to undergo fragmentation.
122
123 ***Senescent fragmentation is seen in vivo in OIS and aging endothelia***
124 To further explore whether SCAFs are a defined structure associated with senescence, we
125 wanted to examine if senescent cells in vivo exhibit features of fragmentation. To address this,
126 we used a model of oncogene-induced senescence in mouse hepatocytes.[21] Here,
127 hydrodynamic tail-vein injection is used to deliver two plasmids, one with transposase and the
128 other carrying a transposon with oncogenic $NRas^{G12V}$-GFP or inactive $NRas^{G12V/D38A}$-GFP. This
129 results in construct expression specifically in individual hepatocytes in the liver [21–23] (Fig. 2A).
130 In this setting, the hepatocytes expressing oncogenic Ras undergo senescence, while the
131 inactive Ras-infected cells remain non-senescent, but in each case the infected cells are GFP-
132 positive. The infected cells can then be identified with immunostaining for GFP, and
133 additionally senescence markers such as SA-β-gal can be used to identify the senescent cells
134 (Fig. 2A).
135
136 Next, on thick sections of liver containing the proliferating control or the senescent
137 hepatocytes, we performed immunostaining and confocal optical-sectioning of GFP,
138 generating image stacks (Fig. 2B). The control cells expressing inactive Ras-GFP clearly
139 retained the epithelial shape of the hepatocytes, whereas the senescent cells displayed a
140 much more irregular, less-circular shape, projecting many branches, as well as scattered non-
141 connecting fragments (Fig. 2B). To determine whether these fragments were indeed separate
142 from the senescent cells, or remained connected, we followed confocal imaging with 3D
143 reconstructions. In each sample analyzed (n=3 livers), SCAFs were detectable adjacent to,
144 but not connected to, the senescent cells, while none were obvious in the controls (Fig. 2C, D;
145 Supplemental Movies 2-3). These results demonstrate that senescent cells *in vivo* generate
146 SCAFs.
147

148 As a second approach to discern whether senescent cells undergo fragmentation in vivo, we
149 investigated age-induced senescent cells, using a recently described senescence-reporter
150 mouse model.[24] Here, p16 positive cells are labeled with GFP, and have been demonstrated
151 to increase in many aged tissues, including in endothelial cells in the liver. Through
152 immunostaining and GFP imaging, we identified numerous GFP-positive senescent
153 endothelial cells in the aged liver, which exhibited characteristics suggestive of cellular
154 fragments (Fig. 2E). Employing confocal optical-sectioning, we were able to confirm that many
155 of these were not physically connected to the senescent cells (Fig. 2F), supporting that
156 senescent cells in aged tissues also undergo fragmentation.
157
158 ***SCAFs contain a variety of organelles including damaged mitochondria***
159 By imaging SCAFs in culture, we observed that these presented as large fragments of
160 senescent cells that formed by attachment to neighboring cells. To further analyze the structure
161 of these bodies, we performed correlative light and electron microscopy (CLEM). We plated
162 senescing GFP-positive cells in an environment of GFP-negative senescing cells (Sen-Sen),
163 and analyzed the cells at 5 days post irradiation. Fluorescence and brightfield imaging allowed
164 us to identify and localize SCAFs of various sizes (Fig. 3A), and these samples were
165 subsequently processed for EM analysis. The same SCAFs were readily identified at the
166 ultrastructural level (Fig. 3B). In each case, the SCAFs appeared as large membrane-bound
167 bodies, filled with cytoplasm. They contained a variety of organelles, including mitochondria,
168 smooth endoplasmic-reticulum, and clathrin vesicles, as well as lipid droplets,
169 autophagosomes and residual bodies (Fig. 3C). In most SCAFs, ribosomes were also clearly
170 visible. In some instances, adherens junctions were visible at the site of adhesion between the
171 SCAF and the neighboring cell, further supporting that SCAFs are generated by cell-cell
172 adhesion (Fig. 3C, D). Quantification of the incidences of the main organelles validated their
173 distribution patterns (Fig. 3E). Interestingly, in all analysis, we were unable to detect nuclei or
174 nuclear material in any of the SCAFs analyzed.
175
176 To further investigate their structure and function, we devised a strategy to collect SCAFs
177 through enzymatic dissociation and fluorescence-activated cell sorting (FACS) isolation (Fig.
178 3F, G). First, we isolated SCAFs and performed cytospin analysis, attaching the GFP-positive
179 cells or SCAFs on glass slides (Fig. 3H). When stained for GFP and with DAPI to detect nuclei,
180 we could not detect DAPI signal in the SCAFs, supporting our EM analysis that SCAFs do not
181 contain nuclear material. Analysis of the size of these sorted SCAFs demonstrated they are
182 similar to those formed in situ in the dilution assay (Extended data Fig. 2). Next,
183 immunostaining for mitochondria, lysosomes and endoplasmic reticulum, again confirmed that
184 in each case, these are frequently found in SCAFs (Fig. 3I).

185
186 Organelle, and in particular mitochondrial damage, has recently been highlighted as a
187 prominent feature in senescent cells, contributing to the SASP.[25,26] Interestingly,
188 immunostaining for p62 foci, a marker of cellular damage and proteotoxic stress showed
189 specific staining in senescent cells and SCAFs (Fig. 3I). Examination of the EM images of
190 SCAFs also identified features of mitochondrial damage including evagination and blebbing
191 (Fig. 3J). Measuring reactive oxygen species (ROS) activity, specifically mitochondrial
192 superoxide, a marker of mitochondrial damage that is elevated in senescent cells, then
193 confirmed the presence of damaged mitochondria (Fig. 3K). Altogether, this uncovers that
194 SCAFs are large pieces of senescent cells, containing damaged organelles, in particular
195 mitochondria, that become adhered to adjacent cells.
196
197 **Disruption of adherens junctions reduces SCAF formation, but increases cell death**
198 A main question is whether SCAFs serve any functional role in senescent cells. To address
199 this, we attempted to inhibit SCAF formation by disrupting adherens junctions. We used siRNA
200 approaches to knockdown *CDH2* (N-cadherin) and *CTNND1* (p120 catenin) in senescent cells
201 (Extended data Fig. 4). Then, GFP-positive senescent cells containing knockdown were diluted
202 into GFP-negative proliferating cells. Quantification by either manual counting or FACS
203 revealed a significant reduction in SCAF-incidence in both cases, demonstrating a functional
204 role for cell-cell adhesion mediated by adherens junctions in the process of SCAF formation
205 (Fig. 4B-D). Unexpectedly however, despite plating equal cell numbers after senescence
206 induction and siRNA transfection, there were fewer cells remaining in the conditions with
207 knockdown compared to siCTR (Fig. 4A). Measurement of cell-viability confirmed that loss of
208 genes that facilitate SCAF formation, causes increased cell death in senescent cells (Fig. 4E),
209 uncovering fragmentation as a protective mechanism in senescent cell survival.
210
211 Mitochondrial damage must be regulated in senescent cells, as excessive damage can trigger
212 cell death.[26] Because we observed that SCAFs contain damaged mitochondria, we asked
213 whether inhibiting SCAF formation would lead to the retention of damaged mitochondria within
214 senescent cells. In control senescent cells, co-staining for mitochondria and ROS revealed
215 detectable mitoSOX foci distributed throughout the cytoplasmic compartment, but with a clear
216 enrichment in forming SCAFs (Fig. 4G). In contrast, cells treated with siCDH2 or siCTNND1
217 displayed visibly elevated mitochondrial ROS within the senescent cell body. Quantification
218 confirmed these observations, with knockdown cells being smaller and accumulating higher
219 levels of both mitochondria and ROS (Fig. 4H). These findings suggest that mitochondrial
220 damage may act as a trigger for SCAF biogenesis.
221

222 To test this possibility, we sought to reduce mitochondrial damage by treating senescent cells
223 with N-acetyl-L-cysteine (NAC), a ROS scavenger known to decrease mitochondrial stress in
224 senescent cells. Strikingly, NAC treatment significantly reduced SCAF formation (Fig. 4I).
225 Finally, to validate our model, we knocked down *CDH2* or *CTNND1* in NAC-treated senescent
226 cells (Fig. 4J). Under conditions of reduced mitochondrial damage, loss of these proteins no
227 longer induced cell death. Together, these results reveal that mitochondrial damage serves as
228 an inducer of SCAF formation, and that SCAFs in turn promote senescent-cell survival by
229 facilitating the removal of damaged organelles.
230
231 ***SCAFs ultimately release their intracellular content, creating cellular debris***
232 As the cell membranes of the SCAFs remain intact during their genesis, we wanted to explore
233 the fate of these structures. To address this, we again sorted SCAFs, and now added them to
234 cultures of proliferating IMR-90 fibroblasts, to track their behavior and dynamics (Extended
235 data Fig. 5A). Interestingly, SCAFs remained intact throughout the procedure, and when plated
236 in culture, they exhibited random dynamic behavior, which included spinning, projecting and
237 retracting arms, or crawling-like behavior (Supplemental Movie 4). To determine how long the
238 SCAFs persisted, we performed quantitative analysis and imaging over time, following their
239 addition to cultures (Extended data Fig. 5B). During the first day, many SCAFs appeared intact,
240 and tended to adhere to the cells in culture. After two days, there was a noticeable decrease
241 in the number of SCAFs, but those remaining still clustered on cells. By three days, most of
242 the GFP signal had disappeared, but any remaining signal was frequently attached to cells, in
243 what appeared to be clusters of cellular debris (Extended data Fig. 5B). Imaging of individual
244 SCAFs at these later timepoints showed that many of them were bursting, or undergoing lysis,
245 and releasing their contents onto the attached cell and into the extracellular environment, while
246 losing GFP-signal (Fig. 5A, Supplemental movies 5-6). To further examine if SCAF rupture
247 generated debris, we repeated the sorting and addition of SCAFs to cultures, but this time
248 adding higher numbers of SCAFs to the recipient cultures. As expected, after 3 days, this
249 clearly resulted in large extra-cellular debris deposits (Fig. 5B).
250
251 This suggests that SCAFs can remain intact for a period of time, but then spill their contents
252 onto the neighboring cells and into the extracellular space, suggesting a novel means of
253 senescent cell communication. Even though GFP-signal was lost upon rupture, we speculated
254 that the intracellular proteins might persist longer. To test this, we used a method to label the
255 protein contents of the senescing cells and the SCAFs. We added L-Homopropargylglycine
256 (L-HPG), a synthetic alternative to methionine that is incorporated during protein translation,
257 and which can then be detected with click-chemistry (Fig. 5C). In this way, the protein content
258 of senescing cells can be subsequently visualized.

259
260 We then diluted GFP-positive senescent cells treated with L-HPG, into GFP-positive L-HPG-
261 negative cultures of proliferating or senescent IMR-90 fibroblasts. Then, these cells were
262 stained using the click-reaction to visualize the L-HPG-labelled proteins, and immuno-stained
263 for GFP and lysosomes (Fig. 5D, E). In each case, SCAFs staining positive for L-HPG were
264 clearly evident, separated from the labeled senescent cells and attached to non-labelled ones.
265 Interestingly, in both settings, intracellular L-HPG staining was evident, presenting as small
266 regular dots, often co-localizing with LAMP1-positive lysosomes, suggesting that some protein
267 from SCAFs was taken up and possibly degraded by the recipient cells (Fig. 5D, E). However,
268 in most cases, the L-HPG labeled proteome from the SCAFs persisted as large extracellular
269 accumulations, attached to the surface of neighboring cells. In many cases, such extracellular
270 deposits were no longer GFP positive, indicating the SCAF had ruptured but its protein content
271 remained as debris on the surface of the cell. This demonstrates that through SCAF formation
272 and subsequent rupture, the intracellular content of senescent cells can be deposited onto, or
273 taken up by, neighboring cells.
274
275 ***The protein content of SCAFs includes DAMPs***
276 The release of intracellular protein and organelles into the microenvironment can have diverse
277 effects, depending on the content. To investigate the protein content of SCAFs that is
278 presumably released upon rupture, we FACS isolated them at two different timepoints (days 5
279 and 10 after irradiation), and performed Mass Spectrometry (MS) analysis (Fig. 6A). This
280 identified the SCAF-associated proteome, revealing strong overlap in protein content among
281 the replicates, and identifying 1376 proteins common to the four replicates (Fig. 6B,
282 Supplemental Table 1). Pathway analysis on these common proteins demonstrated signatures
283 associated with immune cell recruitment and activation, in particular neutrophils, myeloid cells
284 and T-cells (Fig. 6C). In addition, there was pronounced association with both NF-KB and Wnt
285 signaling pathways. When we looked at KEGG pathway association, terms related to cell-cell
286 adhesion appeared, including adherens junction, supporting our earlier findings, and
287 reinforcing the mechanism of formation of SCAFs (Fig. 6D). Curiously, there was a strong
288 association of the protein content with disease, in particular neurodegenerative disease,
289 including Parkinson's disease, Amyotrophic lateral sclerosis, Huntington's and Alzheimer's
290 disease, all situations where senescence has previously been implicated. In order to determine
291 if these signatures were conserved, we also performed similar MS proteomic profiling on
292 SCAFs isolated from mouse dermal fibroblasts (Extended data Fig. 6). Interestingly, many of
293 the same individual proteins and associated signatures seen in human fibroblasts, particularly
294 those relating to neurodegeneration, were also detected.
295

296 When we looked at individual proteins detected in the IMR90 cells, we observed most of the
297 protein components of adherens junctions, including alpha- and beta-catenin, vinculin, VASP
298 and others (Fig. 6E). In addition, there were many membrane proteins that have been
299 associated with immune cell recruitment and senescence including calreticulin, CD44, CD47,
300 and DPP4, a suggested marker of senescent cells [27] (Fig. 6E).We were able to validate our
301 MS findings by immunostaining SCAFs from IMR-90 cells for many of these proteins (Fig. 6F).
302
303 It was also evident that many proteins known as damage-associated molecular patterns
304 (DAMPs) are abundantly present in the SCAFs (Fig. 6G). These include calreticulin, ferritin,
305 multiple Histones, heat shock proteins, cathepsins and high mobility group proteins, among
306 others, findings which were also validated by immunostaining for individual examples on
307 isolated SCAFs (Fig. 6H). This strongly supports that a complex mixture of organelles, as well
308 as intracellular and membrane-associated proteins are released through SCAF formation and
309 rupture.
310
311 ***SCAFs activate cell migration and proliferation in normal and cancer cells***
312 DAMPs play complex biological roles, influencing a variety of cell behaviors, including immune
313 cell activation and recruitment, and cell migration and invasion linked to wound repair. We
314 therefore sought to ask what effect SCAF exposure would have on cells. To address this, we
315 performed RNA-sequencing on cells exposed to SCAFs. We isolated SCAFs from senescent
316 cells and added them to proliferating IMR-90 cells for 20 hours, before sequencing the treated
317 cells (Fig. 7A). Analyzing the RNA sequencing revealed that SCAF treatment resulted in 265
318 genes being significantly upregulated, and 316 genes downregulated (Fig. 7B). Pathway
319 analysis on upregulated differentially expressed genes (DEGs) supported a strong correlation
320 with SCAFs promoting proliferation, migration and invasion, with GO biological process terms
321 such as *wound healing, regulation of cell motility*, *cell population proliferation*, p*ositive*
322 *regulation of cell migration*, and *cell adhesion* associating with the upregulated genes (Fig.
323 7C). Analysis of KEGG associated terms revealed pathways associated with cancer, including
324 *pathways in cancer*, *small cell lung cancer*, and *p53 signaling pathway*. Similar analysis on the
325 downregulated genes further supported these changes, including GO biological process terms
326 like *cell migration*, *cell motility, cell population proliferation* and *response to wounding* (Fig.
327 7D). Supporting this association, genes such as MMP1, MMP14 and MMP16 were induced by
328 SCAFs, while genes for their potential substrates Collagens 1A1, 1A2, 3A1, 4A2, 5A1 and 5A2
329 were decreased.
330
331 To determine whether functional changes were supported by these associations, we examined
332 cells exposed to SCAFs. As expected from the sequencing results, exposure of IMR-90

333 fibroblasts to isolated SCAFs from senescent cells caused significant early increases in
334 proliferation and migration (Fig. 7E, F).
335
336 As the SCAF proteome suggested significant communication with immune cells, we examined
337 how SCAF-exposure would influence macrophages, which are frequently recruited to clear
338 senescent cells.[21] As we had performed for IMR-90 cells, THP1-derived M0 macrophages
339 were exposed to SCAFs and then analyzed by bulk RNA sequencing (Extended data Fig. 7A).
340 Here again, SCAFs activated similar genes and pathways in these cells, associated with
341 migration and motility, but also differentiation, development and cancer (Extended data Fig.
342 7B-D). This further suggests that SCAFs may promote behavioral changes in cells consistent
343 with wound repair.
344
345 As there was such a strong association with cancer signaling and invasion, and given that
346 SCAFs are induced in senescent cancer cells, we also functionally investigated the effects of
347 SCAF-exposure to cancer cells in culture. Here, we found that addition of SCAFs to liver cancer
348 cells in culture also increased proliferation (Fig. 7G). Furthermore, when we added SCAFs to
349 cancer cells in 3D culture, within days, the SCAF-treated cells invaded the gel (Fig. 7H, I). This
350 supports our profiling and demonstrates that SCAFs can promote cell proliferation, migration
351 and invasion in different contexts.
352
353 **DISCUSSION**
354 Here we unveil a previously uncharacterized feature of senescent cells, cellular fragmentation.
355 We have observed the detachment of sizable portions of senescent cells through cell-cell
356 adhesion, coining the term "senescent cell adhesion fragments" (SCAFs). Critically, our
357 investigation has revealed the presence of SCAFs across various senescent cell types in vivo
358 and in vitro, suggesting that SCAFs may serve as additional markers of senescent cells. We
359 identified the mechanism underlying SCAF formation, showing they arise from persistent
360 adherens junction–mediated adhesion of senescent cells to neighboring cells, in the context
361 of cell movement. Surprisingly, and contrary to the view of senescent cells as static, senescent
362 cells in culture are highly dynamic, continuously moving and interacting with surrounding cells.
363 Consistently, in vivo senescence often occurs in contexts of increased cellular dynamics, such
364 as oncogene-induced hyperplasia or wound healing, where various cell types, even
365 hepatocytes, can migrate,[28] suggesting that SCAFs may contribute to these processes.
366
367 The discovery of SCAFs sparks questions into their nature and potential functions. Using
368 various approaches, we identified that SCAFs contain a variety of organelles, including
369 ribosomes, mitochondria and endoplasmic reticulum, and that the mitochondria exhibited

370 typical features of damage previously described in senescent cells.[25,26] However, despite this
371 significant intracellular damage, senescent cells manage to survive, suggesting they have
372 developed ways to tolerate this. This includes the release of mitochondrial DNA and dsRNA
373 into the cytoplasm, preventing mitochondrial-damage associated cell death, but which
374 contributes to SASP activation.[25,26] We propose that that SCAF-mediated disposal of damaged
375 mitochondria is another way of maintaining the level of mitochondrial damage in a tolerable
376 range so as to maintain survival. These findings also introduce the concept that targeting
377 SCAFs could offer a new strategy for eliminating senescent cells in senolytic approaches.
378
379 A major role of the SASP is to recruit immune cells, including macrophages, to clear the
380 senescent cells. Our findings that SCAFs activate pathways of invasion and migration, also in
381 macrophages, supports that this may be a complementary immune-recruitment property along
382 with the SASP, but also initiated by mitochondrial damage. Interestingly, in senescent and
383 damaged cells, damaged mitochondria are shuttled to the cell periphery, raising the possibility
384 that such peripheral localization may favor their inclusion in SCAFs.[26,29] The finding that
385 inhibiting ROS and mitochondrial damage prevents SCAF formation supports such a cross-
386 talk between mitochondrial stress and this adhesion-based fragmentation process.
387
388 Cells have developed various mechanisms to dispose of damaged mitochondria, including
389 migrasomes and exophers. Migrasomes are small, organelle-containing vesicles deposited
390 along the substratum as cells migrate.[29,30] Exophers on the other hand are larger vesicles
391 around 3.5um in diameter, also containing damaged mitochondria and protein aggregates but
392 that are jettisoned to reduce toxicity, as shown in *C. elegans* neurons and mammalian
393 heart.[31,32] While sharing many apparent similarities with SCAFs, including a lack of nuclear
394 material, these features are present in proliferating cells, and neither depends on cell–cell
395 adhesion. SCAFs also appear larger than both. However, further studies directly comparing
396 these structures and formation mechanisms may uncover further similarities or cross-talk, but
397 altogether highlights the variety of complex ways cells have developed to dispose of damaged
398 organelles.
399
400 In addition to uncovering SCAF-related mechanisms and functions, we also investigated the
401 consequences of SCAF formation, uncovering deposition of a complex proteome including
402 DAMPs. DAMPs, also known as alarmins or danger signals, encompass a diverse array of
403 proteins, including heat shock proteins, S100 family members, annexins, histones, and
404 calreticulin, as well as extracellular RNA and membrane lipids.[33–35] When DAMPs become
405 externalized, they promote proliferation, migration, and invasion, recruiting macrophages,
406 neutrophils, and other immune cells, and play pivotal roles in wound repair.[34,36,37] Our pathway

407 analysis of the SCAF proteome and the transcriptional impact of SCAFs on cells aligns with
408 these effects, highlighting the activation of signatures associated with wound repair and
409 immune cell activation, and induction of proliferation, invasion, and migration in exposed cells.
410 DAMPs are also central drivers of inflammaging, a chronic, sterile inflammation underlying
411 many age-related diseases.[34,35,38] As senescent cells are strongly associated with these
412 conditions, the finding that senescent cells continuously dispose of DAMP-rich fragments
413 suggests a direct mechanism by which they may actively fuel this persistent inflammatory
414 state. Indeed, some DAMPs have been identified as SASP components, despite not being
415 secreted via the known secretory pathways,[7,39] suggesting that SCAF formation and rupture
416 may be an additional mechanism by which these proteins are discharged and contribute to the
417 SASP.
418
419 Finally, our study also reveals a robust association between SCAFs and cancer. SCAFs are
420 induced in OIS and therapy-induced senescent cells, and the addition of isolated SCAFs to
421 fibroblasts and cancer cells leads to activation of pathways and properties associated with
422 tumor progression, including proliferation, migration and invasion. How the SCAFs promote
423 these changes remains to be shown, but there are probably multiple factors involved. For
424 example, CD44, present on SCAFs, can induce cancer cell proliferation through direct
425 binding,[40] while numerous DAMPs present in the SCAFs are also linked with cancer
426 progression. We also show that SCAFs induce the expression of collagen-degrading enzymes.
427 As matrix degradation is a primary feature of tumor invasion, there is a compelling rationale to
428 further investigate whether the local production of SCAFs from age-associated or therapy-
429 induced senescent cells could contribute to tumorigenesis and invasion.
430
431 Overall, we believe the identification of SCAFs uncovers yet another exciting feature in the
432 complex biology of senescence, and the ways by which senescent cells interact with their
433 microenvironment. As a core feature of senescent cells, which themselves become detrimental
434 in chronic situations, heightened SCAF formation linked to an increased senescence burden
435 is likely to have adverse effects associated with aging, cancer, neurodegeneration, and other
436 diseases.
437

MATERIALS AND METHODS

Cells

All cells were cultured at 37°C in 5% CO2. IMR-90 cells, used at passages 11 to 15, were cultured in DMEM 41966 + 10% FBS + 100 U/ml penicillin-streptomycin. Huh-7 cells were cultured in RPMI 1640 w/10mM HEPES + 10% FCS + 2.5g/L Glucose + 1mM Sodium Pyruvate + 50 μM β-mercaptoethanol + 40 μg /mL gentamycine. All cell lines were routinely tested for the presence of mycoplasma.

Mouse dermal fibroblast isolation

Primary cultured murine dermal fibroblasts (MDF) were obtained from C57BL/6, $ROSA^{mT/mG}$ (mT/mG) and $APP^{NL-G-F/NL-G-F}$ (APP) P0 pups. Animals were euthanized and the skin was placed in a sterile plastic dish (10 cm diameter), with the dermal side facing the dish, containing 2.5 mg/mL Dispase II (Roche) in PBS and incubated overnight at 4°C. Next day, the epidermis was separated from the dermis. The dermis was subjected to further digestion with 0.25% collagenase A (Roche) in PBS for 30 minutes at 37°C followed by 10 mg/ml DNase for 5 minutes. Dissociated cells were filtered through 70 µm cell strainer to generate a single-cell suspension and then collected by centrifugation and seeded onto 15 cm dishes and cultured in DMEM (4,5g/l glucose) w/GLutamax-I supplemented with 10% Foetal Calf Serum, AANE, 1mM Pyr Na 1 mM, 40 µg/mL gentamycine 100µM β-mercaptoethanol.

THP-1 culture and differentiation into macrophages

THP-1 monocytes were cultured in suspension in RPMI 1640 w 10mM HEPES+ 10% FCS + Glucose 2,5 g/L (14 mM) + Sodium Pyruvate 1 mM + Gentamicine 40 µg/ml. To differentiate them into macrophages, cells were transferred into a culture dish and treated with 200 nM of phorbol 12-myristate 13-acetate for 24 hours, during which time they adhered to the bottom of the dish. After 24 hours, cells were washed in medium and cultured for another 24 hours in normal media. After this, cells were used depending on the experimental setup.

Cell viral transduction

Transduction with retroviral vector was used to generate IMR-90 and Huh-7 cells stably expressing the green fluorescent protein (GFP). Retrovirus was produced by transiently transfecting the Phoenix packaging cell line (G. Nolan, Stanford University, Stanford, CA) with MSCV vector containing GFP coding sequence. Cells were infected with virus for 24 h, drug-selected in 1 µg/mL puromycin for 48 h, and subsequently tested for presence of replicatively competent virus. To generate IMR-90 cells stably expressing GFP and 4-hydroxy tamoxifen inducible ER:ras fusion protein, IMR-90 cells stably expressing GFP were transduced with a retroviral vector encoding the ER:ras protein (Narita, https://www.addgene.org/67844/). Cells were infected with virus for 24 h, selected for 7 days in 500 µg/mL G418 and subsequently tested for presence of replicatively competent virus.

Induction of senescence

For ionizing radiation induced senescence, cells were exposed to a dose of 10 Gy of X-rays using CellRad Precision X-ray irradiator. The device was set to 130 kV and 5 mA at the tray position at one, leading to dose rate of 0.92 Gy/min.

For oncogene induced senescence, cells expressing the ER:ras protein (Young et al., 2009) were exposed to 500nM of 4-hydroxy tamoxifen for the full duration of the experiment.

For therapy induced senescence, IMR-90 cells were treated with 250 nM doxorubicin for 24 hours and Huh-7 cells were treated with 200 nM doxorubicin for 48 hours. Afterwards, the culture was washed and cultured in regular medium. For dilution experiments, senescent cells were diluted in other cells as outlined. For quantification of SCAFs, the number of SCAFs in a given area was counted and expressed as a ratio of the number of senescent cells in the same area at the indicated times. This does not inform if each cell fragments at the same rate, but refers to total incidence at a given time.

493 **SA-ß-Galactosidase staining**
494 IMR-90 stained for SA-ß-Galactosidase activity were washed and fixed in 0.5% glutaraldehyde
495 (Sigma G7651) for 15 minutes at RT. Fixed cells were washed twice with PBS 1X containing
496 1 mM MgCl2 at pH6 and kept at 4°C until SA-ß-Gal experiment (no more than a week). Cells
497 were stained in X-Gal solution consisting of 1 mg/mL X-Gal (Biosynth AG), 5 mM K3Fe(CN)6
498 and 5 mM K4Fe(CN)6 3H2O in PBS1X 1 mM MgCl2 at PH=6 for 8-12 hours. Cells were
499 washed with PBS 1X and imaged with brightfield microscope (EVOS XL Core). SA-B-gal
500 staining on liver tissue was performed on snap-frozen/cryosectioned tissues, that were fixed
501 using glutaraldehyde and then counterstained with Eosin only.
502
503 **Knock-down using siRNA on Doxorubicin-treated IMR-90**
504 siRNA pools of 5 siRNAs for human CDH2 (L-011605-00-0005), human CTNND1 (L-012572-
505 00-0005) and non-targeting control siRNA (D-001810-01-05) were ordered from Dharmacon
506 and were resuspended according to manufacturer's instructions. Cells were seeded at 100,000
507 cells/well in 6-wells plate with 250 nM doxorubicin (Sigma, 44583-1MG) and incubated at 37°C
508 and 5% CO2 for 24 hours. After doxorubicin removal, cells were washed with antibiotic-free
509 medium containing serum. Transfection solution of siRNA and Lipofectamine RNAiMAX
510 (Thermo Fisher 13778075) was prepared in serum-free and antibiotic-free Opti-Mem I and was
511 incubated for 20 min at RT. Cells were then transfected with this solution in antibiotic-free
512 medium for 24 hours, at final concentrations of 25 nM siRNA and 0.25% Lipofectamine. After
513 24 hours, cells were washed with regular medium and grown until desired day.
514
515 **Correlative light and electron microscopy (CLEM)**
516 Fragmenting cells were cultured on laser micro-patterned Aclar supports (1,2). Using a
517 spinning disc confocal microscope (Leica) a time-lapse acquisition was performed, followed
518 by immediate fixation of cells and fragments using 2.5% glutaraldehyde and 2.5%
519 formaldehyde in 0.1M cacodylate buffer for 1 hour at 4°C. After washing, the samples were
520 post-fixed for 1 hour in 1% osmium tetroxide [OsO4] reduced by 0.4% potassium
521 hexacyanoferrate (III) [$K_3Fe(CN)_6$] in H_2O at +4°C. After extensive rinses in distilled water,
522 samples were then stained by 1% uranyl acetate for 1 hour at +4°C, and rinsed in water.
523 Samples were dehydrated with increasing concentrations of ethanol (25%, 50%, 70%, 90%
524 and 3x100%), and embedded with a graded series of epoxy resin. Samples were finally
525 polymerized at 60°C for 48 hours. Ultrathin serial sections (60nm) were picked up on 1%
526 pioloform coated copper slot grids and observed with a Philips CM12 TEM electron microscope
527 (Philips, FEI Electron Optics, Eindhoven, Netherlands) operated at 80kV equipped with an
528 Orius 1000 CDD camera (Gatan, Pleasanton, USA).
529
530 **Fluorescence-Activated Cell Sorting (FACS) isolation**
531 FACS was used to isolate senescent cells and SCAFs. Two million IMR-90 cells stably
532 expressing GFP or mT/mG-MDF cells stably expressing tdTomato and seeded into a p15 petri
533 dish were X-ray irradiated or doxorubicin treated and subsequently cultured for 5-10 days.
534 Before sorting, cells were washed twice with PBS after which 4.5 ml of Accutase (STEMCELL
535 technologies) was added, to dissociate cells and SCAFs and the dish was placed in an
536 incubator. After five minutes cells were gently resuspended using a 5 mL serological pipette
537 and incubated for 5 more minutes. Afterwards, 5.5 mL of 2% FBS in PBS was added and cells
538 were again gently resuspended using 10 mL serological pipette. Then, cells were centrifuged
539 at 290 rcf for 4 minutes. Supernatant was discarded and the pellet resuspended in 3 mL of
540 Pre-Sort Buffer (BD biosciences). Gating for IMR-90 cells was set as in Fig. 4A and similar
541 strategy gating for tdTomato was used for mTmG-MDF cells. Fragments or cells were sorted
542 at RT and collected into 1.5 mL Eppendorf tubes with 350 µl of standard media.
543
544 **Flow-cytometry analysis**
545 For flow-cytometric quantification of SCAFs per cell (FACSquant), cells were first pretreated
546 with Hoechst 33342 in the dish by adding a stock solution to achieve final concentration of 800
547 nM. The dish was returned to the incubator for 20-minute incubation. Afterwards, cells were

processed the same way as for FACS isolation but resuspended in 0.5ml PS buffer in the last step.

Flow-cytometry analysis was performed on BD Symphony under FSC threshold settings of 500. All events were first gated in FSCxSSC to large (cells) and small (debris). Cells were then gated for GFP and Hoechst positivity and GFP+ cells were counted. Debris was then gated for GFP positivity and Hoechst negativity and SCAFs were counted. The gate for GFP positivity was determined beforehand by comparison with GFP- senescent IMR-90 cells. Around 5000 cells were recorded for each analysis.

Flow cytometric analysis for the presence of mitochondria and mitochondrial superoxide radicals in SCAFs was performed in a similar manner as FACSquant. First cells were washed with HBSS (w Ca, Mg), pretreated with mitoSOX Red (1μM) and mitoTracker Deep Red FM (50nM) in HBSS in the incubator for 30 minutes. Then cells were processed and analysed similarly as in FACSquant. The GFP+ SCAFs were then analyzed for mitoSOX (PE-TexasRed) and mitoTracker (APC) signal median fluorescence intensity.

Cytospin

FACS sorted cells or SCAFs were fixed in 4% PFA for 15 minutes at RT and then washed 3x by PBS. Suspension of 150 µL was added into a cytospin funnel mounted on poly-lysine coated microscope slide and centrifuged at 1000 RPM for 5 minutes. Afterwards, the sample was fixed in 4% PFA for 15 minutes at RT, to attach the sample to the slide surface.

Immunofluorescence

Cells/fragments for immunofluorescence were cytospun (see above) or fixed in 4% PFA for 15 minutes at RT followed by 3x PBS wash. Next, the sample was permeabilized for 10 min in PBS + 0.1% Triton-X and washed 3x by PBS. Blocking was done using PBS + 10% goat serum + 0.1% Tween for 1 hour at RT. Primary and secondary antibodies were diluted in PBS +1% goat serum + 0.1% Tween. After blocking, sample was incubated with primary antibody for 1 hour at RT, followed by 3x PBS wash. Then, secondary antibody was added for 1h at RT followed by 3x PBS wash. . Specifically in the case of staining with anti-LAMP1 antibody, the permeabilization, blocking and staining was done with 0.05% saponin (Thermo Scientific, J63209.AK) and without Triton-X or Tween. Subsequently, nuclei were counterstained using DAPI 1 µg/ml for 10 minutes at RT, and actin filaments were counterstained using Phalloidin-AF568 (ThermoFischer) 165 nM. Sample was then washed 3x by PBS and mounted using Fluoromount-G (ThermoFischer).

For immunofluorescent imaging, livers were fixed with 10% neutral buffered formalin for 24 hrs at 4°C and stored in 70% EtOH until further processing. Fixed liver tissues were washed in PBS and sectioned at 100 µm using vibratome. Sections were permeabilized using PBS + 0.5% Triton-X at 4°C overnight. Blocking was done at 4°C for 24 hours in PBS + 10% goat serum + 0.1% Triton-X and primary and secondary antibodies were dissolved in PBS+1% goat serum +0.01% Triton-X. Following blocking, sections were incubated in primary antibody for 24 hours at 4°C, followed by 3x 2-hour wash at 4°C in PBS + 0.01% Triton-X and 24-hour incubation at 4°C with secondary antibody. Afterwards, sections were stained with DAPI 1 µg/ml for 1 hour at 4°C and washed in PBS + 0.01% Triton-X for 3x 2-hours at 4°C. Sections were then mounted on a microscope slide and cleared by serial treatment with 60%, 80% and 87% glycerol for 2 hours per step. Afterwards, samples were mounted in 87% glycerol.

Primary antibodies were used at following concentrations: anti-GFP (1:1000, Abcam, ab13970), anti-DPP4 (1:300, Abcam, ab28340), anti-CTNNB1 (1:500, Abcam, ab16051), anti-CD44 (1:1000, Abcam, ab15710), anti-CD47 (1:1000, BioXcell, MIAP410), anti-ANXA2 (1:500, BD biosciences, 610069), anti-CD166 (1:500, Abcam, ab109215), anti-Histone H4 (1:300, Abcam, ab10158), anti-HSPD1 (1:300, In-House produced, clone: 4MTE-2H7), anti-CALR (1:500, Abcam, ab2907), anti-S100A9 (1:1000, Abcam, ab92507), anti-p62 (1:1000, Abcam, ab109012), anti-LAMP1 (1:300, Abcam, ab24170). Alexa-conjugated secondary antibodies were used in the dilution of 1:1000 – 1:2000.

For mitoSOX Red (1μM; Invitrogen M36008) and mitoTracker Deep Red FM (50nM, Invitrogen M22426), cells were washed with HBSS (w Ca, Mg) and pretreated in the same for 30 minutes at 37°C, 5% CO_2 (incubator). Then cells were washed 3x with HBSS (w Ca, Mg) and imaged in the same medium. Cells were imaged at 37°C, 5% CO_2. MitoSOX Red was imaged using the excitation wavelength of 385nm and the emission was collected with a dsRed filter (592/20 nm).

L-HPG whole proteome labeling

Proliferating GFP labelled IMR-90 cells were treated with 200 μM L-homopropargylglycine (L-HPG) in DMEM without Methionine and cystine medium for 48 hrs. Afterwards, cells were split and reseeded with 250 nm doxorubicin for 24 hours to induce senescence. Then cells were again treated with 200 μM L-HPG in methionine free medium for 48 hrs. Afterwards, cells were trypsinised and diluted/seeded (1:1000) with proliferating or senescent GFP+ IMR-90 cells in glass-bottom dishes. The cells were fixed 5 days after seeding. The click-it staining protocol is the same as for EDU proliferation assay followed by GFP immunostaining (see below and above respectively).

EDU proliferation assay

Cells were incubated with 20 μM of EDU in standard medium for 2 hours. Subsequently, cells were 1x washed with PBS and fixed for 15 minutes in 4% PFA at RT. After fixation, samples were incubated with 100 mM Tris (pH 7.5) for 5 minutes and permeabilized with PBS + 0.1% Triton-X for 10 minutes. Following 3x wash with PBS, cells were stained using Click-staining solution containing either Sulfo-Cy3-Azide or Alexa-Fluor-555-azide for 30 minutes at RT. Subsequently, samples were washed 3x with PBS, stained with DAPI 1 μg/ml for 10 minutes at RT, washed 3x with PBS and mounted using Fluoromount.

MTS assay

Cell viability was measured using CellTiter 96® AQueous Non-Radioactive Cell Proliferation Assay (MTS) (Promega, G5421) according to the manufacturer's instructions.

Time-lapse and confocal microscopy

For acquisition of in-vitro senescent cells and senescent hepatocytes in liver sections, Leica CSU-W1 spinning disk, 63× objective, oil immersion was used with Z step of 0.3 μm.
For confocal images of fragmenting cells Leica SP5 inverted confocal microscope was used with 63x objective, oil immersion.
For live-cell imaging cells were seeded in a 30 mm diameter glass-bottom dish. For acquisition, Zeiss Axio Observer Z1 microscope with 20x dry objective was used. Cells were treated with 30 000 SCAFs and were placed into a humid heated chamber with 5% CO2 and 80% humidity in the microscope. Four positions were selected for each condition and pictures were taken every 5 minutes for 8 hours.

Mass spectrometry analysis of SCAF proteome

After FACS isolation, GFP positive SCAFs from senescent IMR-90 cells were centrifuged at 400g for 5 minutes at room temperature and the pellet was snap-frozen in liquid nitrogen. Same approach with adjusted sorting strategy was used for tdTomato positive SCAFs from senescent MDF cells isolated from mTmG mouse line. Proteins were then precipitated using trichloroacetic acid, followed by acetone wash. Mass spectrometry was performed on Orbitrap Elite using the Top20CIDr method, with 2 hours run and 3 repetitions. Results were analyzed using Proteome Discoverer 1.4 and compared with homo sapiens_181015 database. Thresholds of 1% FDR and minimum of 2 peptides per protein were applied. Pathway analysis was performed using gProfiler (https://biit.cs.ut.ee/gprofiler/gost). Gene Ontology Databases and KEGG biological pathway database were considered. Adjusted p-value of <0.05 was used as a threshold to select the significant enrichment.

658
659 **RNA sequencing of SCAF treated cells**
660 Proliferating GFP negative IMR-90 cells were treated with 300 000 SCAFs or inert beads for
661 20 hours under normal culture conditions. Four independent biological replicates per condition
662 were generated. The same approach was used for THP-1 derived macrophages, which were
663 done in three biological replicates per condition. Cells were washed 1x with PBS and lysed in
664 350 µl of Guanidine thiocyanate-based lysis buffer (LBP lysis buffer, Macherey-Nagel
665 NucleoSpin RNA plus isolation kit, Ref. 740984), RNA was isolated and sent to the GenomEast
666 platform at Institut de Génétique et de Biologie Moléculaire et Cellulaire (IGBMC). Library was
667 prepared using TruSeq Stranded mRNA Library preparation (Illumina). Sequencing was
668 performed with HiSeq 4000 technology (Illumina) on single-end 50bp length reads. Reads
669 were pre- processed to remove low quality and short (<40bp) reads using cutadapt v1.10.
670 Remaining reads were mapped onto the hg38 assembly of Homo sapiens genome using STAR
671 version 2.5.3a. Gene expression quantification was performed from uniquely aligned reads
672 using htseq-count version 0.6.1p1, with annotations from Ensembl version 98 and "union"
673 mode. Read counts have been normalized across samples with the median-of-ratios method
674 proposed by Anders and Huber, to make these counts comparable between samples.
675 Differential gene expression analysis was performed using Wald test, as proposed by Love et
676 al. and implemented in the Bioconductor package DESeq2 version 1.16.1. P-values were
677 adjusted for multiple testing using the Benjamini and Hochberg method. Genes with an
678 adjusted p-value <0.05 were considered significantly differentially expressed. Pathway
679 analysis was performed using gProfiler (https://biit.cs.ut.ee/gprofiler/gost). Gene Ontology
680 Databases and KEGG biological pathway database were considered. Adjusted p-value of
681 <0.05 was used as a threshold to select the significant enrichment.
682
683 **Cell motility assay**
684 Proliferating IMR-90 cells were seeded in a 4 chamber 30 mm diameter glass-bottom dish
685 (IBL, Ref 220.120.022) with 8000 cells per chamber. For acquisition, Zeiss Axio Observer Z1
686 microscope with 20x dry objective was used. Cells were treated with Hoechst 33342 0.5 µg/ml,
687 30 000 SCAFs or inert beads and were placed into a humid heated chamber with 5% CO2 and
688 80% humidity in the microscope. Four positions were selected for each condition and pictures
689 were taken for 8 hours every 5 minutes. Cell nuclei were automatically detected using StarDist
690 and subsequently tracked using the TrackMate ImageJ modules.
691
692 **Focus formation assay**
693 Huh-7 cells were seeded into 6 well plates in two different densities – 2000 cells and 4000
694 cells per well. At 24 and 48 hours after seeding, cells were treated either by normal medium
695 or by 60 000 SCAFs isolated from senescent IMR-90 cells expressing GFP. After 10 days,
696 cells were fixed in 4% PFA at RT for 15 minutes and washed with PBS. Subsequently, cells
697 were stained with crystal violet using a standard protocol.
698
699 **Spheroid Matrigel-invasion assay**
700 To generate spheroids derived from Huh-7 cells, 40 000 cells were seeded into Ultra-low
701 adhesion 96 well plates (Corning). After 48 hours, formed spheroids were treated either with
702 standard medium or 30 000 SCAFs. Plate was then centrifuged at 300g for 5 minutes.
703 Supernatant was aspirated and spheroids were embedded in Matrigel +10% rat tail collagen.
704 Spheroids were imaged daily using a 5x dry objective. Eight technical replicates were
705 performed in each independent experiment. On day 8, the area of visible outgrowth was
706 manually traced and measured.
707
708 **Statistical analysis**
709 Unless otherwise specified, results from each group were averaged and expressed as means
710 + standard error of the mean (SEM) (represented as error bars). T-test was used for
711 comparison between 2 groups and one-way ANOVA analysis was used for comparisons
712 among 3 or more groups. Two-way ANOVA analysis was used to examine the influence of two

different independent variables. The Statistics program Prism (GraphPad Prism 9) was used for analysis.

REFERENCES

1. Muñoz-Espín, D. & Serrano, M. Cellular senescence: from physiology to pathology. *Nat Rev Mol Cell Biol* **15**, 482–496 (2014).
2. Rhinn, M., Ritschka, B. & Keyes, W. M. Cellular senescence in development, regeneration and disease. *Development* **146**, dev151837 (2019).
3. Childs, B. G. *et al.* Senescent cells: an emerging target for diseases of ageing. *Nat Rev Drug Discov* **16**, 718–735 (2017).
4. Gorgoulis, V. *et al.* Cellular Senescence: Defining a Path Forward. *Cell* **179**, 813–827 (2019).
5. Schmitt, C. A., Wang, B. & Demaria, M. Senescence and cancer — role and therapeutic opportunities. *Nat Rev Clin Oncol* **19**, 619–636 (2022).
6. Coppé, J.-P., Desprez, P.-Y., Krtolica, A. & Campisi, J. The senescence-associated secretory phenotype: the dark side of tumor suppression. *Annu Rev Pathol* **5**, 99–118 (2010).
7. Basisty, N. *et al.* A proteomic atlas of senescence-associated secretomes for aging biomarker development. *PLoS Biol* **18**, e3000599 (2020).
8. Birch, J. & Gil, J. Senescence and the SASP: many therapeutic avenues. *Genes Dev.* **34**, 1565–1576 (2020).
9. Kang, T. W. *et al.* Senescence surveillance of pre-malignant hepatocytes limits liver cancer development. *Nature* **479**, 547–551 (2011).
10. Ritschka, B. *et al.* The senescence-associated secretory phenotype induces cellular plasticity and tissue regeneration. *Genes Dev.* **31**, 172–183 (2017).
11. Demaria, M. *et al.* An Essential Role for Senescent Cells in Optimal Wound Healing through Secretion of PDGF-AA. *Developmental Cell* **31**, 722–733 (2014).
12. Mosteiro, L. *et al.* Tissue damage and senescence provide critical signals for cellular reprogramming in vivo. *Science* **354**, aaf4445 (2016).
13. Xu, M. *et al.* Senolytics improve physical function and increase lifespan in old age. *Nat Med* **24**, 1246–1256 (2018).
14. Baker, D. J. *et al.* Naturally occurring p16Ink4a-positive cells shorten healthy lifespan. *Nature* **530**, 184–189 (2016).
15. Bussian, T. J. *et al.* Clearance of senescent glial cells prevents tau-dependent pathology and cognitive decline. *Nature* **562**, 578–582 (2018).
16. Chinta, S. J. *et al.* Cellular Senescence Is Induced by the Environmental Neurotoxin Paraquat and Contributes to Neuropathology Linked to Parkinson's Disease. *Cell Rep* **22**, 930–940 (2018).
17. Schafer, M. J. *et al.* Cellular senescence mediates fibrotic pulmonary disease. *Nat Commun* **8**, 14532 (2017).
18. Demaria, M. *et al.* Cellular Senescence Promotes Adverse Effects of Chemotherapy and Cancer Relapse. *Cancer Discov* **7**, 165–176 (2017).
19. Zhang, P. *et al.* Senolytic therapy alleviates Aβ-associated oligodendrocyte progenitor cell senescence and cognitive deficits in an Alzheimer's disease model. *Nat Neurosci* **22**, 719–728 (2019).
20. Zhang, L., Pitcher, L. E., Prahalad, V., Niedernhofer, L. J. & Robbins, P. D. Targeting cellular senescence with senotherapeutics: senolytics and senomorphics. *The FEBS Journal* **290**, 1362–1383 (2023).
21. Kang, T.-W. *et al.* Senescence surveillance of pre-malignant hepatocytes limits liver cancer development. *Nature* **479**, 547–551 (2011).
22. Chan, A. S. L. *et al.* Titration of RAS alters senescent state and influences tumour initiation. *Nature* **633**, 678–685 (2024).

23. Yin, K. *et al.* Senescence-induced endothelial phenotypes underpin immune-mediated senescence surveillance. *Genes Dev* **36**, 533–549 (2022).
24. Grosse, L. *et al.* Defined p16High Senescent Cell Types Are Indispensable for Mouse Healthspan. *Cell Metab* **32**, 87-99.e6 (2020).
25. López-Polo, V. *et al.* Release of mitochondrial dsRNA into the cytosol is a key driver of the inflammatory phenotype of senescent cells. *Nat Commun* **15**, 7378 (2024).
26. Victorelli, S. *et al.* Apoptotic stress causes mtDNA release during senescence and drives the SASP. *Nature* **622**, 627–636 (2023).
27. Kim, K. M. *et al.* Identification of senescent cell surface targetable protein DPP4. *Genes Dev.* **31**, 1529–1534 (2017).
28. Matchett, K. P. *et al.* Multimodal decoding of human liver regeneration. *Nature* **630**, 158–165 (2024).
29. Jiao, H. *et al.* Mitocytosis, a migrasome-mediated mitochondrial quality-control process. *Cell* **184**, 2896-2910.e13 (2021).
30. Ma, L. *et al.* Discovery of the migrasome, an organelle mediating release of cytoplasmic contents during cell migration. *Cell Res* **25**, 24–38 (2015).
31. Melentijevic, I. *et al.* C. elegans neurons jettison protein aggregates and mitochondria under neurotoxic stress. *Nature* **542**, 367–371 (2017).
32. Nicolás-Ávila, J. A. *et al.* A Network of Macrophages Supports Mitochondrial Homeostasis in the Heart. *Cell* **183**, 94-109.e23 (2020).
33. Huang, J. *et al.* DAMPs, ageing, and cancer: The 'DAMP Hypothesis'. *Ageing Res Rev* **24**, 3–16 (2015).
34. Franceschi, C., Garagnani, P., Vitale, G., Capri, M. & Salvioli, S. Inflammaging and 'Garb-aging'. *Trends Endocrinol Metab* **28**, 199–212 (2017).
35. Franceschi, C. & Campisi, J. Chronic inflammation (inflammaging) and its potential contribution to age-associated diseases. *J Gerontol A Biol Sci Med Sci* **69 Suppl 1**, S4-9 (2014).
36. Vénéreau, E., Ceriotti, C. & Bianchi, M. E. DAMPs from Cell Death to New Life. *Front Immunol* **6**, 422 (2015).
37. Hernandez, C., Huebener, P. & Schwabe, R. F. Damage-associated molecular patterns in cancer: a double-edged sword. *Oncogene* **35**, 5931–5941 (2016).
38. Furman, D. *et al.* Chronic inflammation in the etiology of disease across the life span. *Nat Med* **25**, 1822–1832 (2019).
39. Davalos, A. R. *et al.* p53-dependent release of Alarmin HMGB1 is a central mediator of senescent phenotypes. *J Cell Biol* **201**, 613–629 (2013).
40. Dhar, D. *et al.* Liver Cancer Initiation Requires p53 Inhibition by CD44-Enhanced Growth Factor Signaling. *Cancer Cell* **33**, 1061-1077.e6 (2018).

ACKNOWLEDGEMENTS

This work was supported by grants from La Fondation pour la Recherche Medicale (FRM) Amorcage pour les jeunes equipes (AJE20160635985), and Programme "Maladies Neurodégénératives 2020" (MND202004011743) ; Fondation ARC pour la Recherche sur le Cancer (PJA20181208104) ; IDEX Attractivité - University of Strasbourg (IDEX2017) ; La Fondation Schlumberger pour l'Education et la Recherche FSER 19 (Year 2018)/FRM ; Agence Nationale de la Recherche (ANR) ANR-19-CE13- 0023-03 and ANR-22-CE14-0062-01 ; la Fondation pour la Recherche sur Alzheimer (2024) ; and Ligue Contre le Cancer (all to W.M. K.). The work was also supported by an institutional grant to the IGBMC, ANR-10-LABX-0030-INRT, a French State fund managed by the Agence Nationale de la Recherche under the frame program Investissements d'Avenir ANR-10-IDEX-0002-02. Sequencing was performed by the GenomEast platform, a member of the "France Genomique" consortium (ANR-10- INBS-0009). We acknowledge the support of the Light Microscopy Facility at the IGBMC imaging center, member of the national infrastructure France-BioImaging supported by the French National Research Agency (ANR-10-INBS-04). The funders had no role in study

design, data collection and analysis, decision to publish, or preparation of the manuscript. We thank Katerina Jerabkova-Roda for valuable feedback on the work and sharing resources.

FIGURE LEGENDS

Figure 1. Cells undergoing senescence form cell-cell adhesion dependent fragments.

(A) Experimental design of live cell imaging of individual GFP-labelled cells undergoing senescence.

(B) GFP, phase contrast (PH) and DAPI images of cells diluted as per the scheme in A, on day 5 after plating. Arrowheads indicate GFP containing cellular fragments in the cultures with senescent cells (Scale bar = 80 μm)

(C) Confocal image of senescent cell (green) diluted in GFP-negative cells, shows GFP fragments adhere to the membrane of adjacent cells in Sen-Sen condition. (Scale bar = 80 μm)

(D) Timelapse imaging of GFP senescent cells diluted in GFP-negative proliferating cells at Day 3. Asterisk labels the adhesion point between cells. Arrowhead labels senescent fragment formation (Scale bar = 80 μm)

(E) Quantification of fragments per cell at different time-points after senescence induction, in each culture condition. (Data are mean ± SEM, n = 3-5. One-way ANOVA, Dunnett's multiple comparison test.)

(F) Confocal micrographs (maximum Z-projection) of 4 different regions of interest (ROI) reveal the size and shape of senescent fragments. Top row shows anti-GFP immunostaining (green). Bottom row shows composites of chromatin (DAPI - cyan) and actin (phalloidin – magenta) staining and anti-GFP immunostaining (green). (Scale bar = 40 μm.)

(G) Measurement of major axis length of fragments in cell-dilution cultures. (Red line indicates the mean of major axis length of all fragments, n=2327. Measurements were acquired from 3 biological replicates.)

(H) Experimental design of live cell imaging of individual GFP-labelled senescent cells. GFP, phase contrast (PH) and DAPI images of individually plated cells (Scale bar = 40 μm). Graph shows quantification of number of fragments per cell (salmon bars show the same results as in E for reference, n = 3-4).

(I) Images of cell-dilution strategy using oncogene induced senescence (OIS) in human primary lung fibroblasts (IMR-90) and irradiation- (IIS) and therapy- (TIS) induced senescence in human hepatocyte-derived carcinoma cell line (Huh7). (Scale bar = 80 μm, GFP, green; DAPI, blue)

Figure 2. SCAFs are present in oncogene-induced senescent mouse hepatocytes and aging-induced senescent liver endothelial cells in vivo.

(A) Hematoxylin Eosin (H&E), SA-B-gal staining and GFP immunostaining were performed on liver sections 6 days after hydrodynamic tail-vein mediated delivery of active $Nras^{G12V}$ (OIS – oncogene induced senescence), or inactive $Nras^{G12V/D38A}$ (CTR) and GFP coding sequences.

(B) Maximum Z-projection confocal images of control (CTR, $Nras^{G12V/D38A}$) and senescent (OIS, $Nras^{G12V}$) hepatocytes expressing GFP. (GFP, green; DAPI, blue). Insets i and ii indicate regions of the image used for 3D rendering in the IMARIS software. (Scale bar = 80 μm) Graph shows quantification of cell circularity (Data are mean ± SEM, n = 3. Student's t-test.)

(C) IMARIS rendering of control hepatocytes (CTR, $Nras^{G12V/D38A}$). (Scale bar = 20 μm)

(D) IMARIS rendering of senescent hepatocytes (OIS, $Nras^{G12V}$). White arrowheads indicate SCAFs not connected to senescent cell. (i scale bar = 10 μm, ii scale bar = 8 μm.)

(E) Maximum Z-projection confocal image of senescent liver endothelial cells in one year old p16 reporter mice (p16-Cre/ROSA-mT/mG). Numbered arrows indicate SCAFs shown in F. (Scale bar = 80 μm)

(F) Orthogonal views of SCAFs selected in E. (Scale bar = 5μm)

Figure 3. SCAFs are large membrane bound bodies containing damaged organelles.
(A) Brightfield and GFP-image of live-cell microscopy of GFP-senescent cell dilution model. Numbers indicate individual SCAFs later imaged by TEM.
(B) Low magnification TEM image of the region of interest shown in A. Four GFP positive SCAFs are indicated. (Scale bar = 1 µm.)
(C) Higher magnification of GFP positive SCAFs 1-4 from B. (AJ, adherens junction: SER, smooth endoplasmic reticulum: M, mitochondria: LD, lipid droplet: RB, residual body: AP, autophagosome: R, ribosomes. Scale bar for 1,2 and 3 = 1 µm; for 4 is 0.5 µm.)
(D) Additional SCAF showing adherens junction. (AJ, adherens junction: RB, residual body, AP, autophagosome: M, mitochondria. Scale bar = 1 µm.)
(E) Percentage of SCAFs containing the indicated organelles (n=30).
(F) and (G) Experimental design and gating of fluorescence-activated cell sorting of intact, GFP positive senescing cells and SCAFs (SCAF-FACS).
(H) Cytospin and immunostaining of senescent cells and SCAFs for GFP (green) with DAPI staining of DNA (cyan). (Scale bar = 80 µm)
(I) SCAF-FACS followed by cytospin combined with various staining approaches to visualize organelles present in senescent cells and SCAFs. Graphs indicate the proportion of cells/SCAFs containing the specified organelle. (n = 3, Scale bar = 80 µm)
(J) Aberrant mitochondria are present in SCAFs as seen by CLEM. Arrows in left indicate a residual body and concentric laminated mitochondria with mitochondrial wall disruptions. Arrow in the right indicates a mitochondrial vacuole. (Scale bars = 1 µm and 0.5 µm respectively.
(K) Graphs indicate the presence of mitochondria (MitoTracker) and mitochondria derived superoxide (MitoSOX) in FACS-analysed SCAFs. (n = 6, Mann-Whitney test)

Figure 4. Knockdown of adherens junction (AJ) components in senescent cells attenuates SCAF formation and leads to reduced cell viability.
(A) Whole-coverslip low-magnification scan of the GFP signal (black) in the cell-dilution model with adherens junction components knockdown: GFP+ IMR-90 cells induced to senesce (doxorubicin – DOXO), followed by siRNA treatment, were seeded with GFP- proliferating IMR-90 cells onto coverslips in equivalent numbers. Coverslips were stained and imaged 5 days after seeding. (Scale bars = 2mm.)
(B) Higher magnification images from the samples shown in A (DNA – blue, GFP – green). siCDH2 (N-cadherin knockdown) and siCTNND1 (p120 knockdown) show reduced SCAF burden and smaller cell size after AJ components knockdown. (Scale bars = 80 µm.)
(C) Quantification of SCAF formation by IF staining and manual counting on day 5 after seeding. (Data are mean ± SEM, n = 3. One-way ANOVA, Dunnett's multiple comparison test.)
(D) Quantification of SCAF formation by FACS analysis of the number of SCAFs and cells on day 5 after seeding. (Data are mean ± SEM, n = 3. One-way ANOVA, Dunnett's multiple comparison test.)
(E) Measurement of cell viability 4 days after siRNA transfection of senescent cells, using aqueous formazan-based colorimetric assay – MTS.
(F) Experimental design of live cell imaging of mitochondria (mitoTracker) and mitochondrially produced superoxide (mitoSOX). Imaging is performed 4 days after siRNA transfection.
(G) siCDH2 and siCTNND1 show striking differences in distribution and amount of mitoTracker (magenta) and mitoSOX (green) signal (GFP – blue) comp. Quantification in H. (Scale bars = 80 µm.)
(H) Quantification of cell area and mean fluorescent intensities of mitoTracker and mitoSOX. (Data are mean ± SEM, n = 4. One-way ANOVA, Dunnett's multiple comparison test.)
(I) Quantification of SCAF formation by FACS analysis of the number of SCAFs and cells on day 5 after senescence induction. N-acetyl-L-cysteine treatment with indicated concentration was commenced right after induction and maintained until measurement. (Data are mean ± SEM, n = 3. One-way ANOVA, Dunnett's multiple comparison test.)
(J) Manual quantification of the number of cells per field of view (10 fields per condition) on day 5 after siRNA transfection. 1 mM N-acetyl-L-cysteine treatment rescues the cell loss

caused by siCDH2 (and siCTNND1). (Data are mean ± SEM, n = 3. Two-way ANOVA, Šídák's multiple comparison test – only indicated comparisons were performed.)

Figure 5. SCAFs maintain their integrity for a limited time after which they rupture, release their cytoplasmic content and form cellular debris.
(A) Timeframe images of GFP positive (green) SCAF rupture and debris generation. Arrowheads indicate SCAFs at different time-points. (Scale bar = 10 μm)
(B) Brightfield imaging at days (D) 1 and 3 after adding increasing number of SCAFs to culture generating increased cell debris (arrowheads). (Scale bar = 80 μm) Graph represents the quantification of the total debris area on day 3. (Data are mean ± SEM, n = 3. One-way ANOVA, Dunnett's multiple comparison test.)
(C) Experimental design of senescent cell nascent proteome labeling using L-homopropargyl glycine (L-HPG) shown in D and E.
(D) and (E) Spinning-disc confocal imaging of L-HPG labelled GFP+ cells diluted in non-labelled GFP+. (DAPI – blue, GFP – green, L-HPG – magenta, LAMP1 – yellow.) In (D) labelled senescent are seeded with non-labelled proliferating cells. In (E) labelled senescent cells are seeded with non-labelled senescent cells. Orthogonal views of different channels are shown to demonstrate the distribution of the SCAF-derived material on the surface of, or inside of neighboring cells. (Scale bars = 80 μm)

Figure 6. SCAFs contain proteins associated with innate immune processes, age-related diseases and contain Damage Associated Molecular Patterns (DAMPs).
(A) Experimental design of Mass Spectrometry (MS) analysis of the protein content of SCAFs isolated from senescent IMR-90 cells.
(B) Overlap of proteins identified in SCAFs by MS. (S1, sample 1; S2, sample 2; D5, day 5; D10, day 10).
(C) Bioinformatic analysis of SCAF proteome using gProfiler (GO Biological process) reveals strong association with immune-related processes and signaling.
(D) Bioinformatic analysis of SCAF proteome using gProfiler (KEGG pathway) reveals strong association with multiple age-related degenerative diseases.
(E) Tables indicating protein components of adherens junction complexes and representative cell surface proteins detected in SCAF-proteome.
(F) Immunofluorescence for representative surface marker proteins in isolated SCAFs. (Scale bar = 80 μm)
(G) Table listing DAMP proteins detected in SCAF-proteome.
(H) Immunofluorescence for selected DAMP proteins in isolated SCAFs. (Scale bar = 80 μm)

Figure 7. SCAFs promote proliferation, cell migration, and invasion of cancer cells.
(A) Experimental design of RNA sequencing analysis of primary human fibroblast (IMR-90) after 20 hours of SCAF exposure.
(B) Volcano plot of differentially expressed genes between IMR-90 cells treated with SCAFs compared to control cells treated with inert beads of similar size.
(C) Bioinformatic analysis of significantly upregulated genes after SCAF-exposure using gProfiler. GO Biological process and KEGG pathway terms are shown.
(D) Bioinformatic analysis of significantly downregulated genes after SCAF-exposure using gProfiler. GO Biological process and KEGG pathway terms are shown.
(E) EDU incorporation assay at different time points (D, days) after SCAF-exposure in IMR90 fibroblasts. (Small dots indicate positivity of each field of view, colors represent biological replicates. Bordered dots indicate the mean of an experiment. Bars are mean ± SEM of proliferation relative to control cells on day 0. Two-way ANOVA, Šídák's multiple comparison test – only indicated comparisons were performed.)
(F) Cell motility measurement after SCAF-exposure in IMR-90 fibroblasts, relative to inert bead treated controls. (Small symbols represent median velocity of a single nucleus, colors indicate

biological replicates. Bordered symbols show the mean of an experiment. Bars are mean ± SEM of the median velocity. Paired t-test.)
(G) Focus formation assay of human hepatocyte-derived carcinoma cell line (Huh-7) on day 14 after treatment with SCAFs or medium on day 0 and day 2. Graph shows the quantification of the integrated density of the red channel of the whole well. (Data are mean ± SEM, n = 3, unpaired t-test.)
(H) Huh-7 spheroid Matrigel-invasion assay after SCAFs or medium treatment. (Scale bar = 1 mm)
(I) Quantification of Huh-7 invasion of Matrigel, measured as the outgrowth area of spheroids from H on day 8. (Small symbols represent outgrowth area of a single spheroid, colors indicate biological replicates. Bordered symbols show the mean of an experiment. Bars are mean ± SEM of the outgrowth area. Unpaired t-test.)

Supplementary Figure 1. The dynamics of senescence features in irradiation-induced senescence.
(A) Time-course of the expression of $p21^{CIP1}$ after senescence induction in IMR90 cells. (Data are mean ± SEM, n = 3. One-way ANOVA, Dunnett's multiple comparison test.)
(B) Time-course of the expression of $p16^{INK4A}$ after senescence induction in IMR90 cells. (Data are mean ± SEM, n = 3-4. One-way ANOVA, Dunnett's multiple comparison test.)
(C) Time-course of SA-B-gal positivity after senescence induction in IMR90 cells.

Supplementary Figure 2. Average major-axis length of FACS-isolated senescent cells and SCAFs.

Supplementary Figure 4. Validation of siRNA approaches targeting adherens junction components
(A) Relative mRNA levels of CDH2 gene targeted by the corresponding siRNA. Normalized to Rplp0 and no-siRNA. n=1
(B) Relative mRNA levels of CTNND1 gene targeted by the corresponding siRNA. Normalized to Rplp0 and no-siRNA. n=1
(C) Western blot for N-cadherin (encoded by the CDH2 gene) and Tubulin after targeting with 25 nM siRNA. n=1

Supplementary Figure 5. FACS isolated SCAFs maintain their integrity for several days.
(A) Image of living GFP positive (green) SCAFs isolated by FACS and seeded on top of proliferating GPF-negative IMR-90 cells. (Scale bar = 80 µm)
(B) Representative images of GFP positive (green) SCAFs at different times (Days0-3) after seeding on proliferating GPF negative IMR-90 cells. Arrowheads indicate residual GFP positive SCAFs surrounded by GFP negative cellular debris. (Scale bar = 80 µm)

Supplementary Figure 6. Mass Spectrometry analysis of the protein content of SCAFs isolated from senescent mouse dermal fibroblast (MDF) cells.
(A) Overlap of proteins identified in MDF derived SCAFs by MS.
(B) Bioinformatic analysis of MDF SCAF proteome using gProfiler (GO Biological process) reveals strong association with immune-related processes and signaling.
(C) Bioinformatic analysis of MDF SCAF proteome using gProfiler (KEGG pathway) reveals strong association with multiple age-related degenerative diseases.

Supplementary Figure 7. SCAF-treatment of THP-1 derived macrophages promotes cell migration and signaling pathways regulating macrophage activation.
(A) Experimental design of RNA sequencing analysis of THP-1 derived macrophages after 20 hours of SCAF exposure.
(B) Volcano plot of differentially expressed genes between macrophage cells treated with SCAFs compared to control cells treated with inert beads of similar size.

1041 (C) Bioinformatic analysis of significantly upregulated genes after SCAF-exposure using
1042 gProfiler. GO Biological process and KEGG pathway terms are shown.
1043 (D) Bioinformatic analysis of significantly downregulated genes after SCAF-exposure using
1044 gProfiler. GO Biological process and KEGG pathway terms are shown.
1045
1046 **Supplementary Table 1. SCAF Proteome**
1047 List of the proteins that were identified in each of the replicate isolations of SCAFs that were
1048 analyzed by Mass Spectrometry.
1049
1050

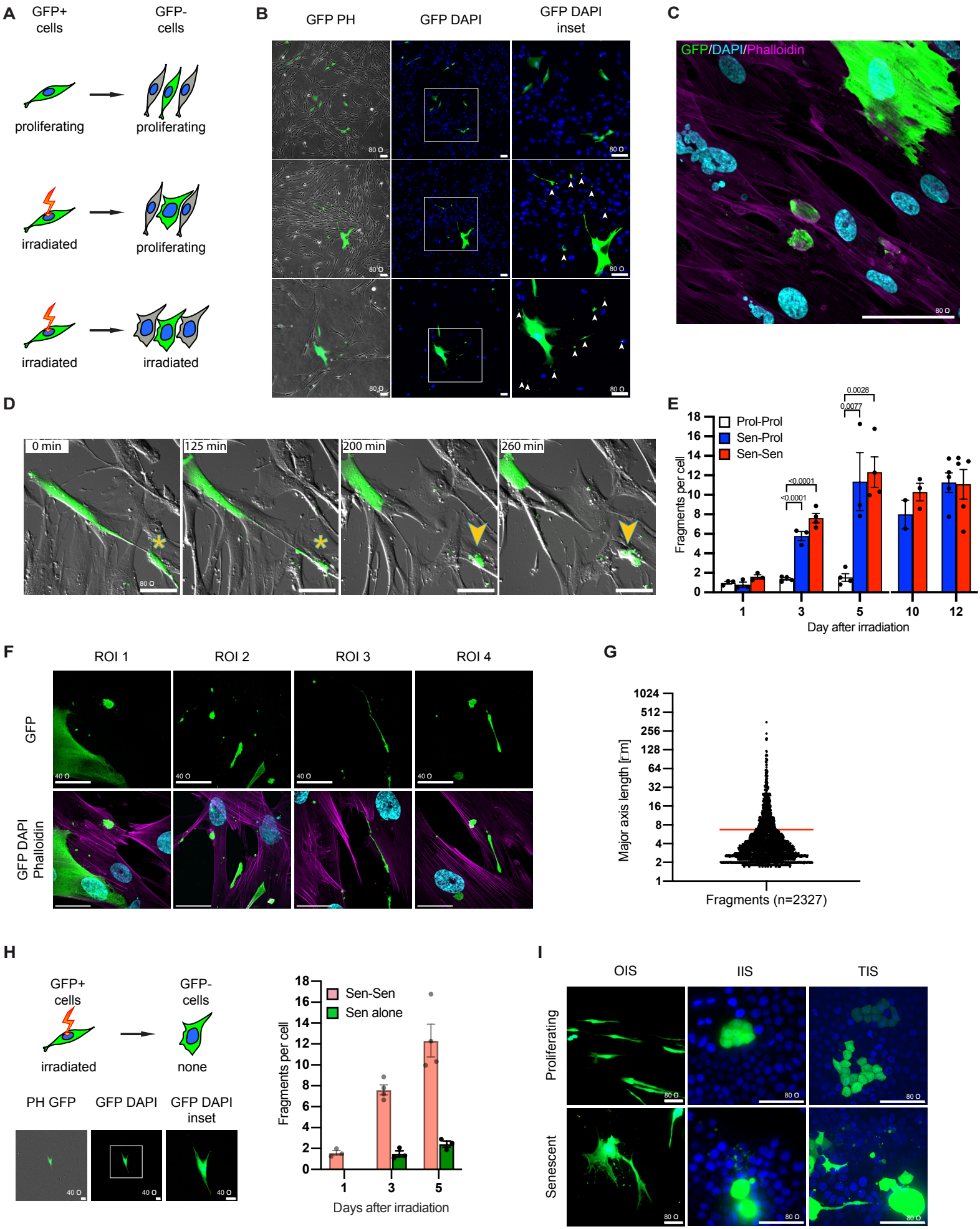
A
GFP+ cells
GFP- cells
proliferating
proliferating
irradiated
proliferating
irradiated
irradiated
B
GFP PH
GFP DAPI
GFP DAPI inset
C
GFP/DAPI/Phalloidin
D
0 min
125 min
200 min
260 min
E
Prol-Prol
Sen-Prol
Sen-Sen
Fragments per cell
Day after irradiation
<0.0001
<0.0001
0.0077
0.0028
F
ROI 1
ROI 2
ROI 3
ROI 4
GFP
GFP DAPI Phalloidin
G
Major axis length [µm]
Fragments (n=2327)
H
GFP+ cells
GFP- cells
irradiated
none
PH GFP
GFP DAPI
GFP DAPI inset
Sen-Sen
Sen alone
Fragments per cell
Days after irradiation
I
OIS
IIS
TIS
Proliferating
Senescent

Fig1

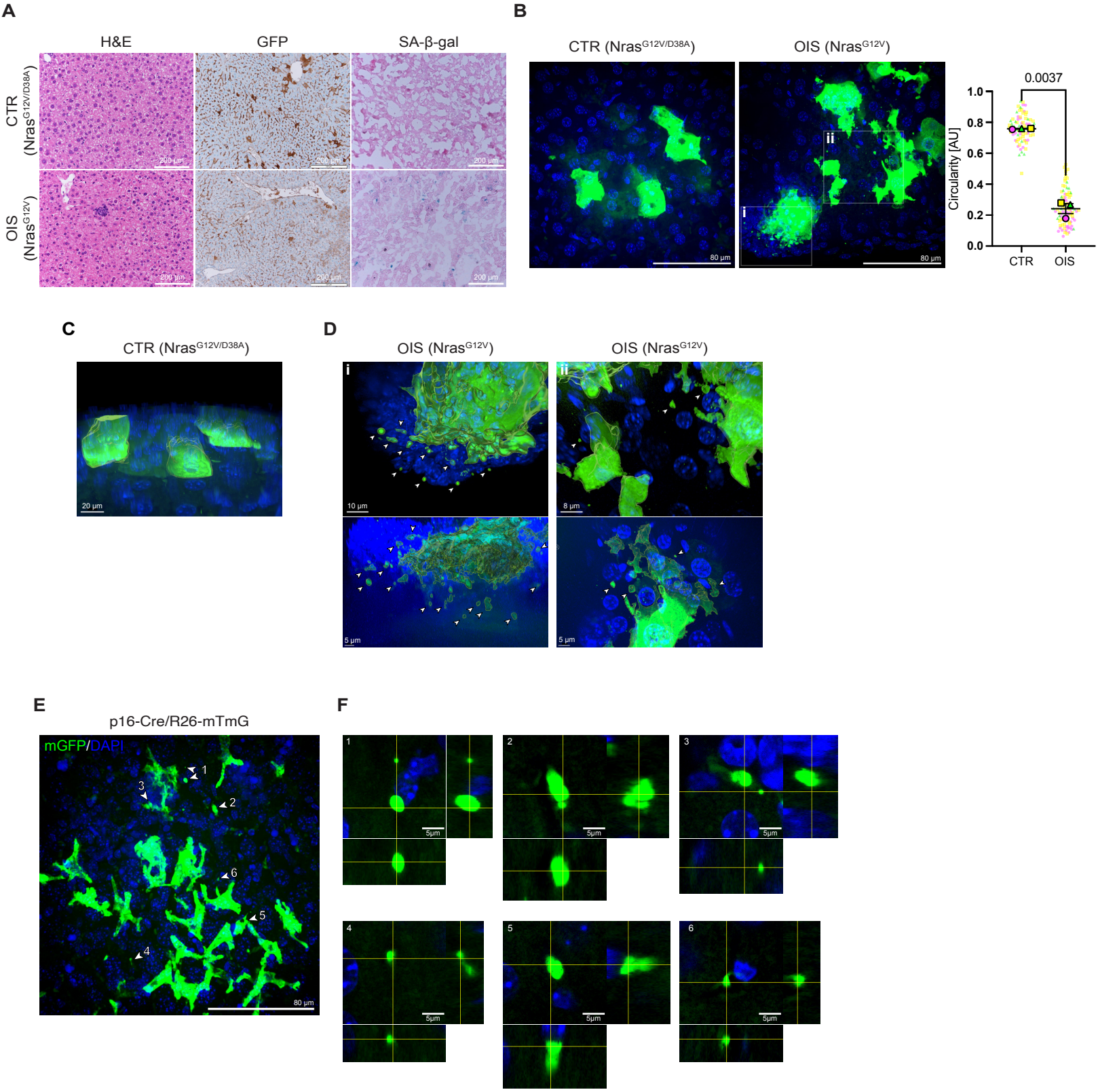
A
H&E
GFP
SA-β-gal
CTR (NrasG12V/D38A)
OIS (NrasG12V)
200 µm
B
CTR (NrasG12V/D38A)
OIS (NrasG12V)
i
ii
80 µm
0.0037
Circularity [AU]
1.0
0.8
0.6
0.4
0.2
0.0
CTR
OIS
C
CTR (NrasG12V/D38A)
20 µm
D
OIS (NrasG12V)
OIS (NrasG12V)
10 µm
8 µm
5 µm
E
p16-Cre/R26-mTmG
mGFP/DAPI
1
2
3
4
5
6
80 µm
F
5µm

Fig2

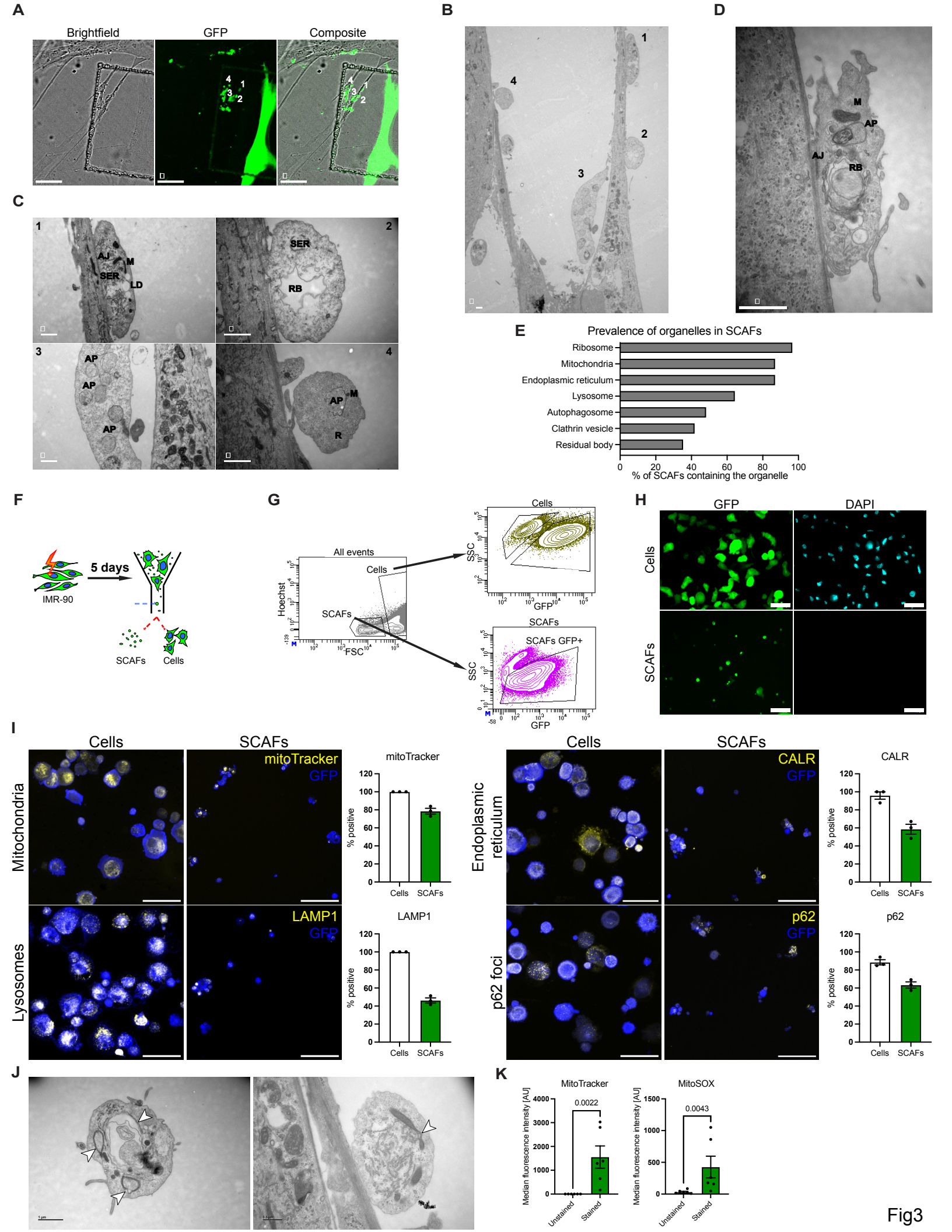
A
Brightfield
GFP
Composite
B
C
AJ
M
SER
LD
RB
AP
R
D
E
Prevalence of organelles in SCAFs
Ribosome
Mitochondria
Endoplasmic reticulum
Lysosome
Autophagosome
Clathrin vesicle
Residual body
% of SCAFs containing the organelle
F
5 days
IMR-90
SCAFs
Cells
G
All events
Hoechst
FSC
SSC
GFP
SCAFs GFP+
H
GFP
DAPI
I
Cells
SCAFs
mitoTracker
LAMP1
CALR
p62
Mitochondria
Lysosomes
Endoplasmic reticulum
p62 foci
% positive
J
K
MitoTracker
MitoSOX
Median fluorescence intensity [AU]
0.0022
0.0043
Unstained
Stained

Fig3

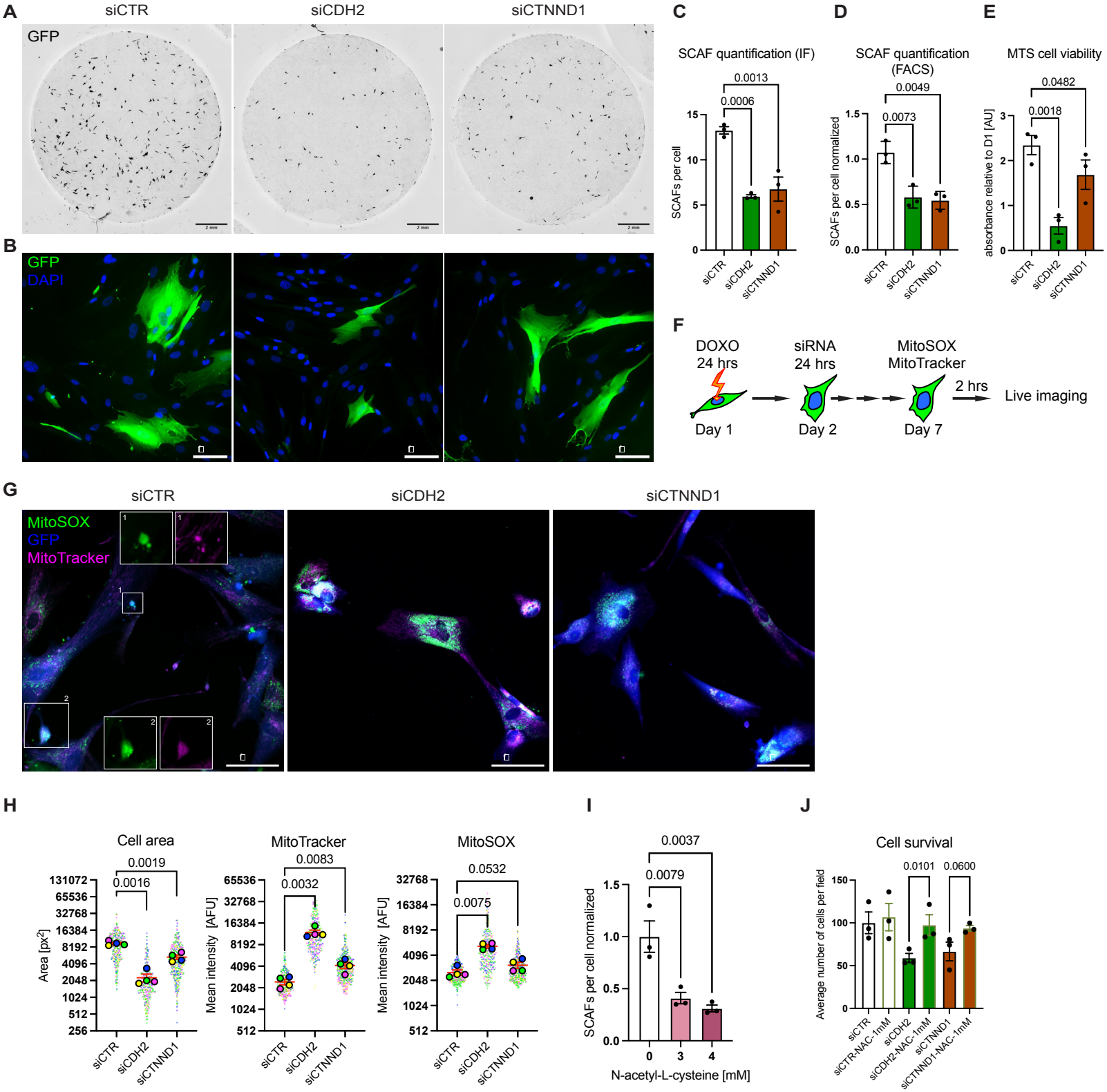
A
siCTR
siCDH2
siCTNND1
GFP
B
GFP
DAPI
C
SCAF quantification (IF)
SCAFs per cell
0.0013
0.0006
D
SCAF quantification (FACS)
SCAFs per cell normalized
0.0049
0.0073
E
MTS cell viability
absorbance relative to D1 [AU]
0.0482
0.0018
F
DOXO 24 hrs
siRNA 24 hrs
MitoSOX MitoTracker
2 hrs
Live imaging
Day 1
Day 2
Day 7
G
siCTR
siCDH2
siCTNND1
MitoSOX
GFP
MitoTracker
H
Cell area
Area [px²]
0.0019
0.0016
MitoTracker
Mean intensity [AFU]
0.0083
0.0032
MitoSOX
Mean intensity [AFU]
0.0532
0.0075
I
SCAFs per cell normalized
0.0037
0.0079
N-acetyl-L-cysteine [mM]
J
Cell survival
Average number of cells per field
0.0101
0.0600
siCTR-NAC-1mM
siCDH2-NAC-1mM
siCTNND1-NAC-1mM

Fig4

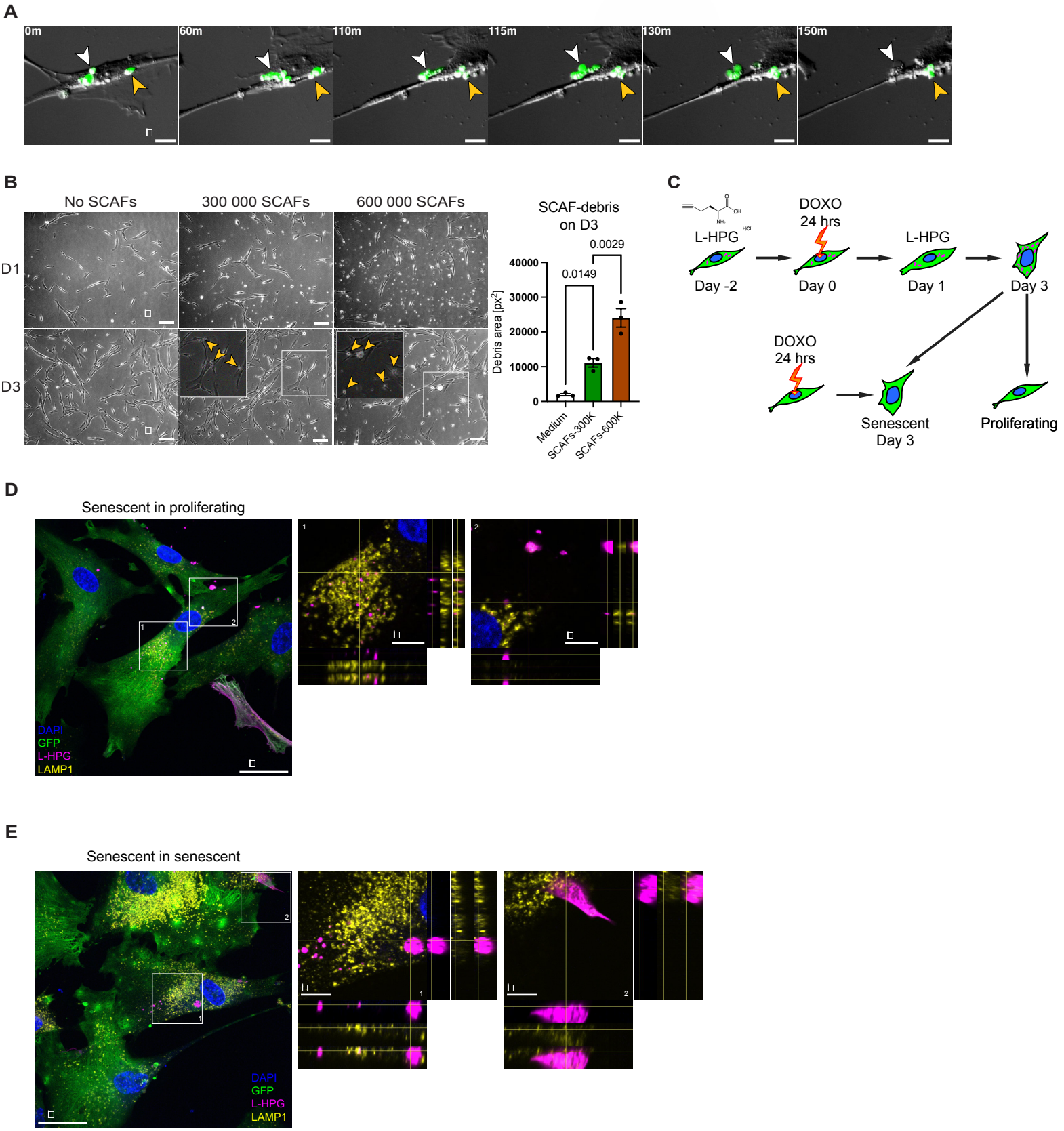
A
0m
60m
110m
115m
130m
150m
B
No SCAFs
300 000 SCAFs
600 000 SCAFs
D1
D3
SCAF-debris on D3
0.0149
0.0029
Debris area [px²]
40000
30000
20000
10000
0
Medium
SCAFs-300K
SCAFs-600K
C
L-HPG
DOXO 24 hrs
L-HPG
Day -2
Day 0
Day 1
Day 3
DOXO 24 hrs
Senescent Day 3
Proliferating
D
Senescent in proliferating
DAPI
GFP
L-HPG
LAMP1
E
Senescent in senescent
DAPI
GFP
L-HPG
LAMP1

Fig5

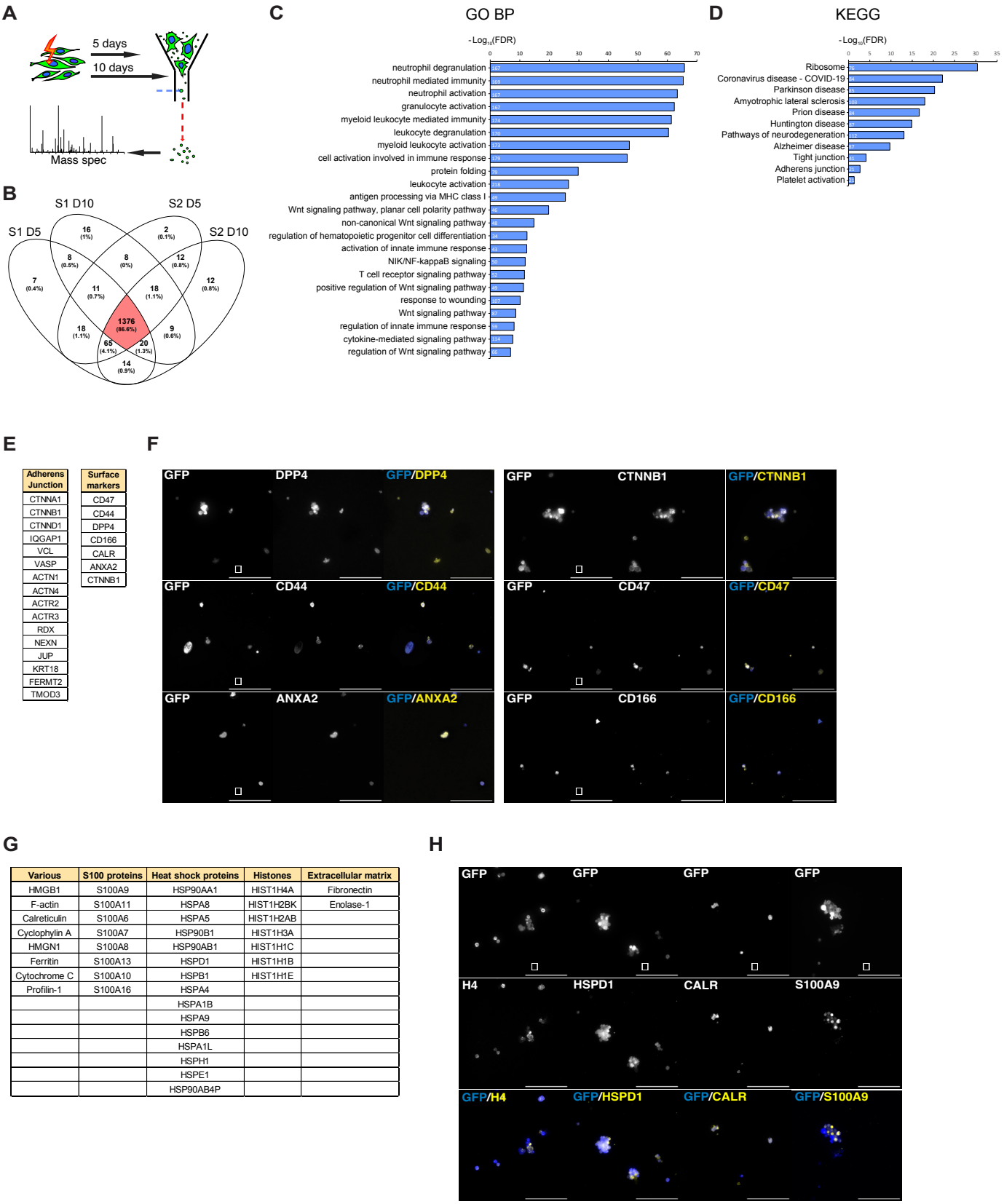

Various	S100 proteins	Heat shock proteins	Histones	Extracellular matrix
HMGB1	S100A9	HSP90AA1	HIST1H4A	Fibronectin
F-actin	S100A11	HSPA8	HIST1H2BK	Enolase-1
Calreticulin	S100A6	HSPA5	HIST1H2AB	
Cyclophylin A	S100A7	HSP90B1	HIST1H3A	
HMGN1	S100A8	HSP90AB1	HIST1H1C	
Ferritin	S100A13	HSPD1	HIST1H1B	
Cytochrome C	S100A10	HSPB1	HIST1H1E	
Profilin-1	S100A16	HSPA4		
		HSPA1B		
		HSPA9		
		HSPB6		
		HSPA1L		
		HSPH1		
		HSPE1		
		HSP90AB4P		

Fig6

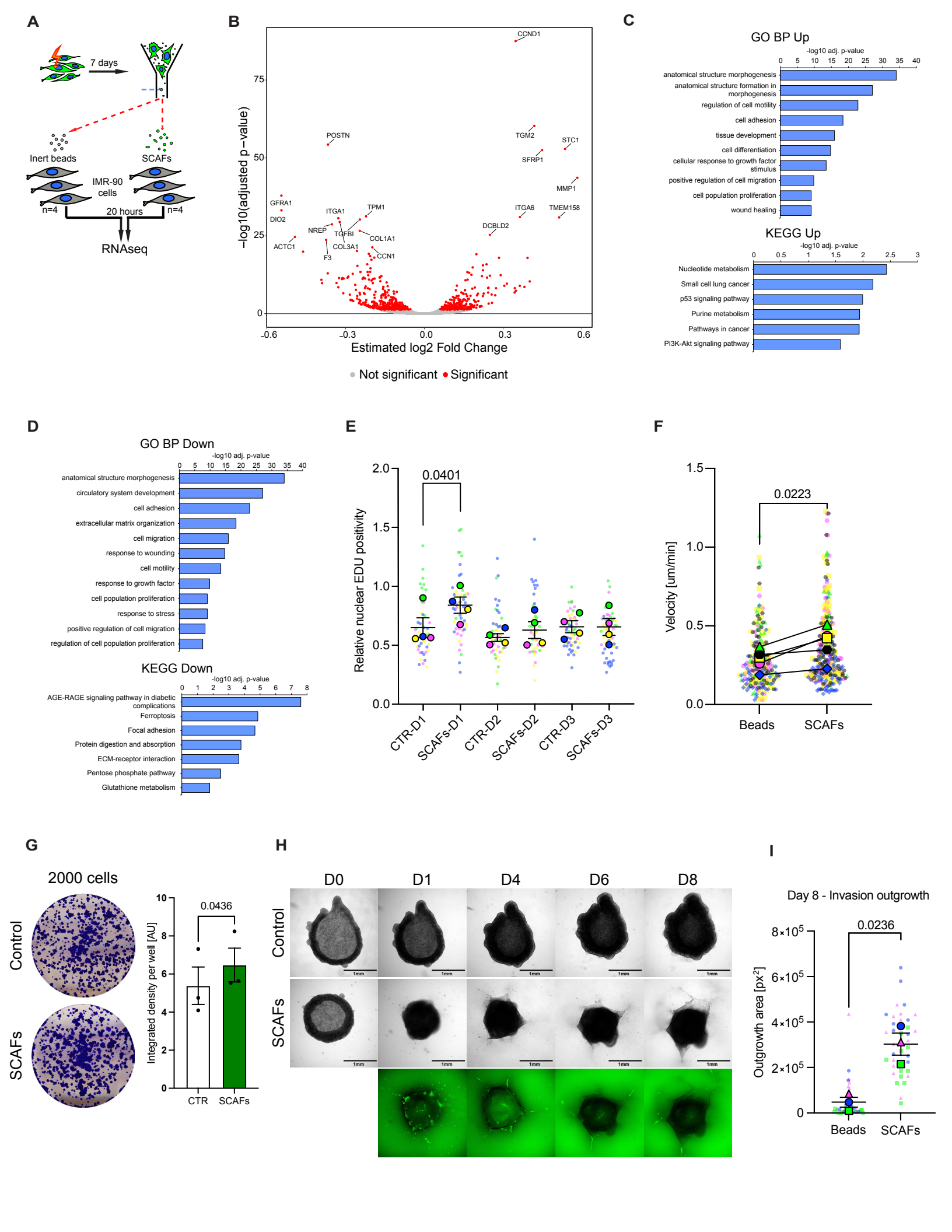
A
7 days
Inert beads
SCAFs
IMR-90 cells
n=4
n=4
20 hours
RNAseq
B
CCND1
POSTN
TGM2
STC1
SFRP1
MMP1
GFRA1
DIO2
ITGA1
TPM1
NREP
TGFBI
COL1A1
COL3A1
ACTC1
F3
CCN1
ITGA6
TMEM158
DCBLD2
−log10(adjusted p−value)
Estimated log2 Fold Change
Not significant
Significant
C
GO BP Up
-log10 adj. p-value
anatomical structure morphogenesis
anatomical structure formation in morphogenesis
regulation of cell motility
cell adhesion
tissue development
cell differentiation
cellular response to growth factor stimulus
positive regulation of cell migration
cell population proliferation
wound healing
KEGG Up
-log10 adj. p-value
Nucleotide metabolism
Small cell lung cancer
p53 signaling pathway
Purine metabolism
Pathways in cancer
PI3K-Akt signaling pathway
D
GO BP Down
-log10 adj. p-value
anatomical structure morphogenesis
circulatory system development
cell adhesion
extracellular matrix organization
cell migration
response to wounding
cell motility
response to growth factor
cell population proliferation
response to stress
positive regulation of cell migration
regulation of cell population proliferation
KEGG Down
-log10 adj. p-value
AGE-RAGE signaling pathway in diabetic complications
Ferroptosis
Focal adhesion
Protein digestion and absorption
ECM-receptor interaction
Pentose phosphate pathway
Glutathione metabolism
E
0.0401
Relative nuclear EDU positivity
CTR-D1
SCAFs-D1
CTR-D2
SCAFs-D2
CTR-D3
SCAFs-D3
F
0.0223
Velocity [um/min]
Beads
SCAFs
G
2000 cells
Control
SCAFs
0.0436
Integrated density per well [AU]
CTR
SCAFs
H
D0
D1
D4
D6
D8
Control
SCAFs
1mm
I
Day 8 - Invasion outgrowth
0.0236
Outgrowth area [px²]
Beads
SCAFs

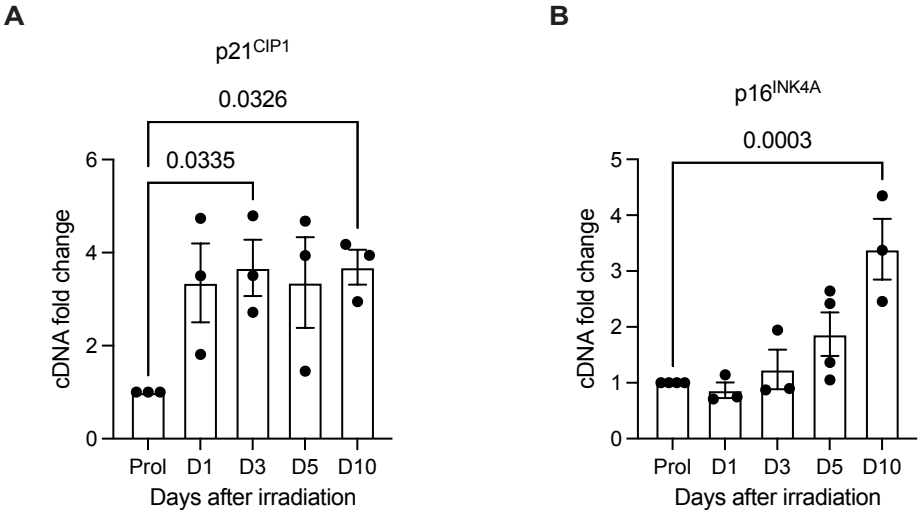
A
p21CIP1
0.0326
0.0335
cDNA fold change
0
2
4
6
Prol
D1
D3
D5
D10
Days after irradiation
B
p16INK4A
0.0003
cDNA fold change
0
1
2
3
4
5
Prol
D1
D3
D5
D10
Days after irradiation

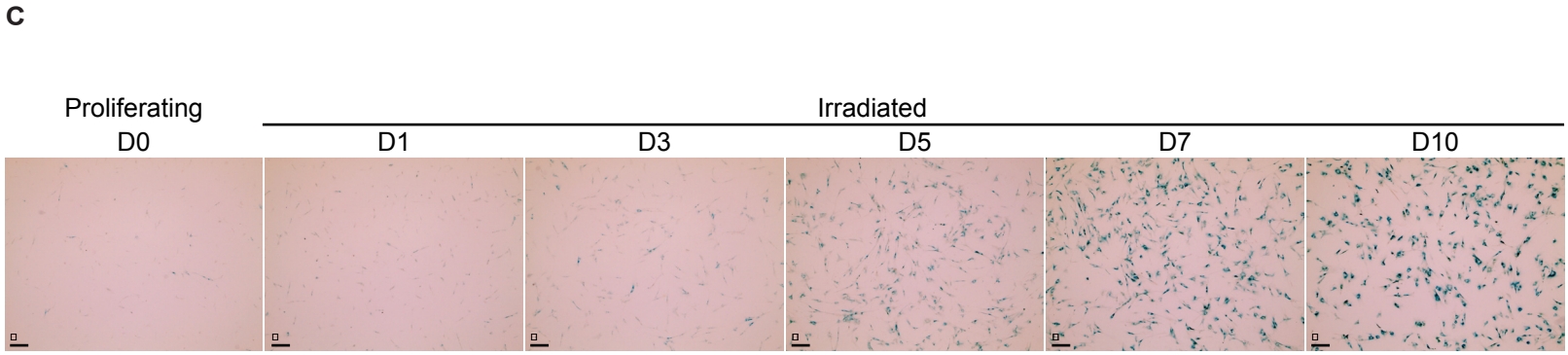
C
Proliferating
Irradiated
D0
D1
D3
D5
D7
D10

FigS1

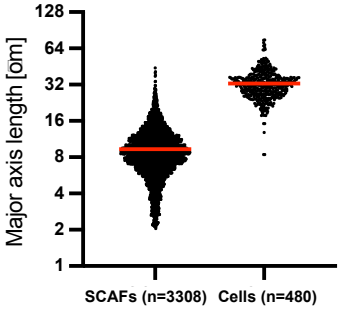

FigS2

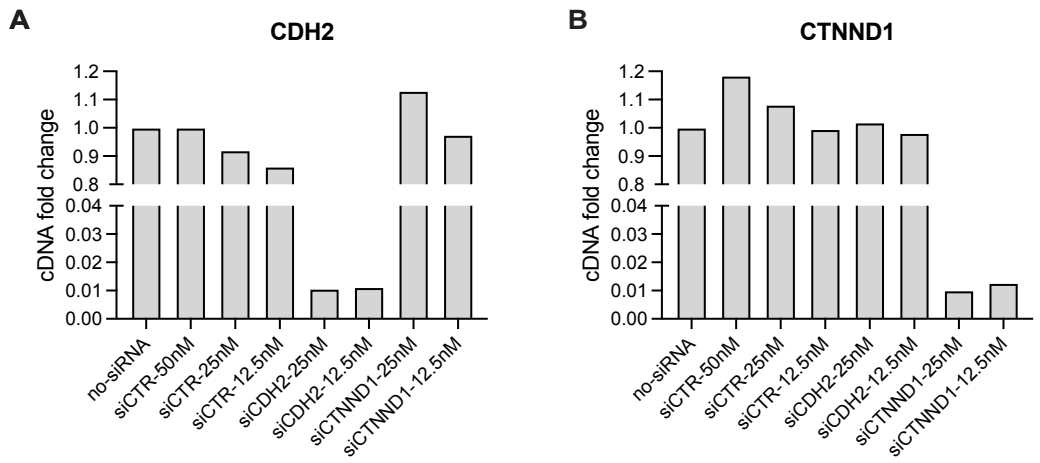
A
CDH2
cDNA fold change
1.2
1.1
1.0
0.9
0.8
0.04
0.03
0.02
0.01
0.00
no-siRNA
siCTR-50nM
siCTR-25nM
siCTR-12.5nM
siCDH2-25nM
siCDH2-12.5nM
siCTNND1-25nM
siCTNND1-12.5nM
B
CTNND1
cDNA fold change
1.2
1.1
1.0
0.9
0.8
0.04
0.03
0.02
0.01
0.00
no-siRNA
siCTR-50nM
siCTR-25nM
siCTR-12.5nM
siCDH2-25nM
siCDH2-12.5nM
siCTNND1-25nM
siCTNND1-12.5nM

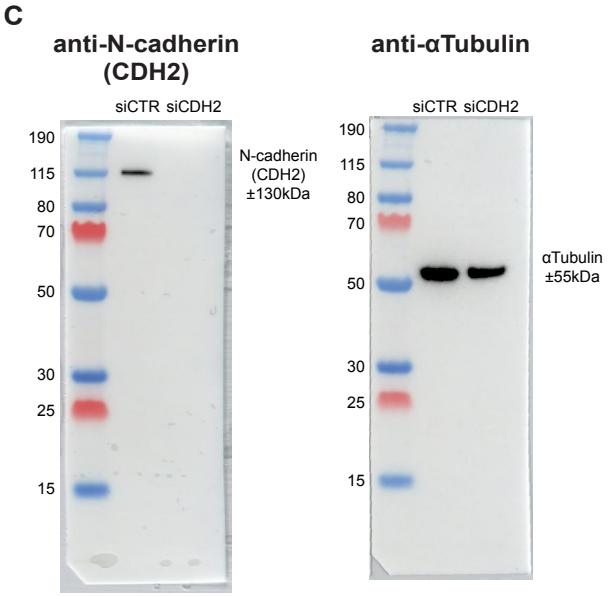
C
anti-N-cadherin
(CDH2)
siCTR siCDH2
190
115
80
70
50
30
25
15
N-cadherin
(CDH2)
±130kDa
anti-αTubulin
siCTR siCDH2
190
115
80
70
50
30
25
15
αTubulin
±55kDa

FigS4

A

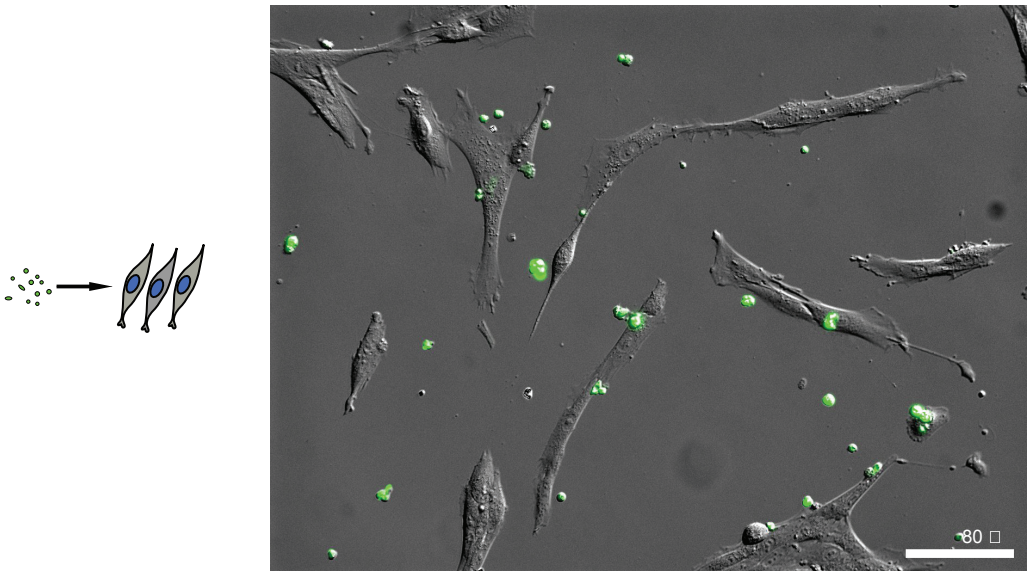

B

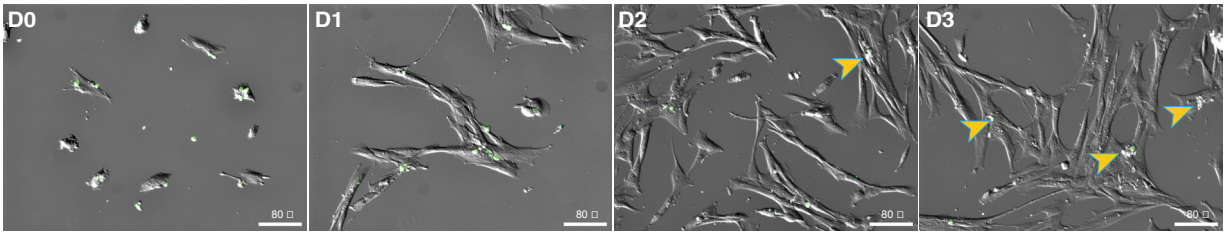

FigS5

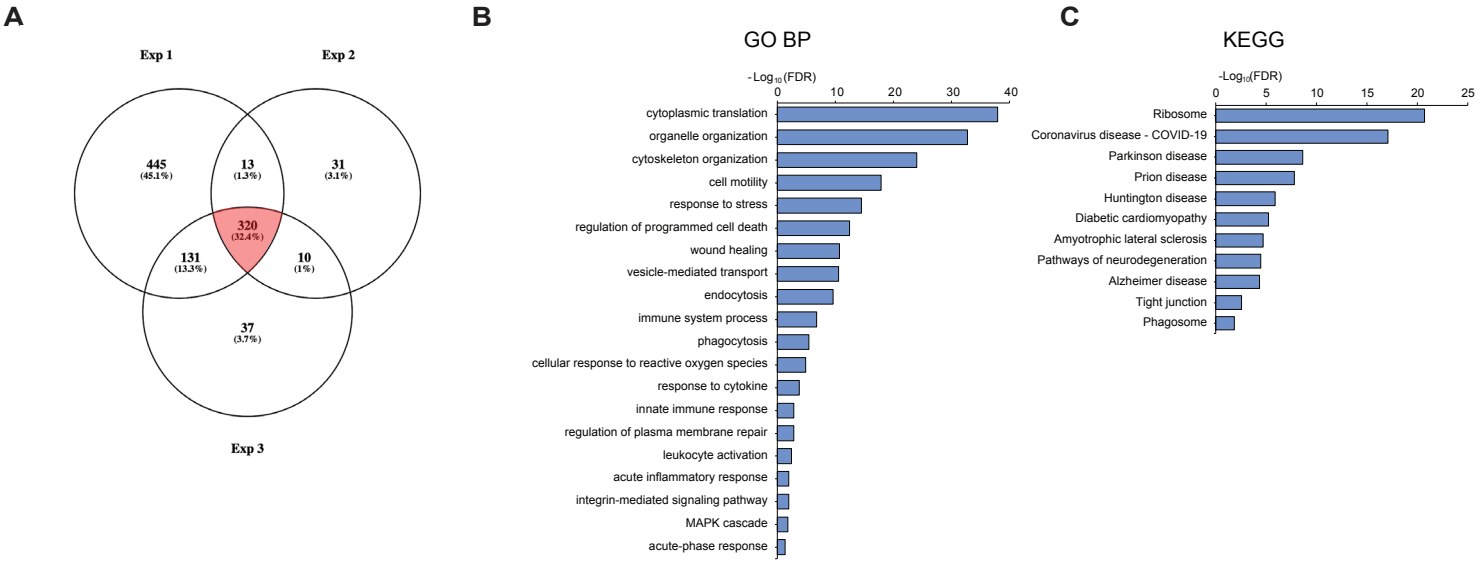
A
Exp 1
Exp 2
Exp 3
445
(45.1%)
13
(1.3%)
31
(3.1%)
320
(32.4%)
131
(13.3%)
10
(1%)
37
(3.7%)
B
GO BP
-Log10(FDR)
0
10
20
30
40
cytoplasmic translation
organelle organization
cytoskeleton organization
cell motility
response to stress
regulation of programmed cell death
wound healing
vesicle-mediated transport
endocytosis
immune system process
phagocytosis
cellular response to reactive oxygen species
response to cytokine
innate immune response
regulation of plasma membrane repair
leukocyte activation
acute inflammatory response
integrin-mediated signaling pathway
MAPK cascade
acute-phase response
C
KEGG
-Log10(FDR)
0
5
10
15
20
25
Ribosome
Coronavirus disease - COVID-19
Parkinson disease
Prion disease
Huntington disease
Diabetic cardiomyopathy
Amyotrophic lateral sclerosis
Pathways of neurodegeneration
Alzheimer disease
Tight junction
Phagosome

FigS6

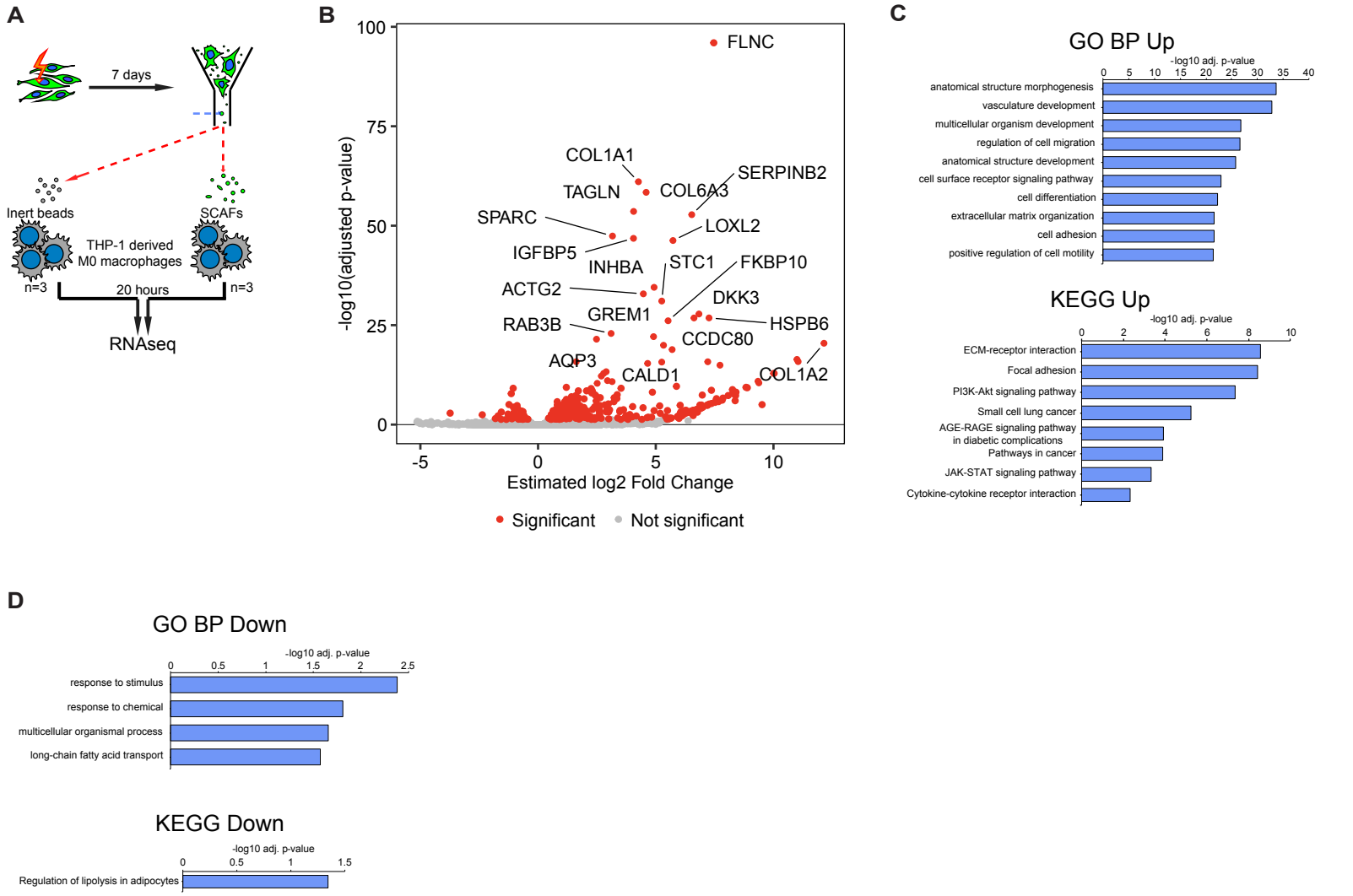
A
7 days
Inert beads
SCAFs
THP-1 derived
M0 macrophages
n=3
n=3
20 hours
RNAseq
B
FLNC
COL1A1
SERPINB2
TAGLN
COL6A3
SPARC
LOXL2
IGFBP5
INHBA
STC1
FKBP10
ACTG2
DKK3
GREM1
RAB3B
HSPB6
CCDC80
AQP3
CALD1
COL1A2
-log10(adjusted p-value)
Estimated log2 Fold Change
Significant
Not significant
C
GO BP Up
-log10 adj. p-value
anatomical structure morphogenesis
vasculature development
multicellular organism development
regulation of cell migration
anatomical structure development
cell surface receptor signaling pathway
cell differentiation
extracellular matrix organization
cell adhesion
positive regulation of cell motility
KEGG Up
-log10 adj. p-value
ECM-receptor interaction
Focal adhesion
PI3K-Akt signaling pathway
Small cell lung cancer
AGE-RAGE signaling pathway in diabetic complications
Pathways in cancer
JAK-STAT signaling pathway
Cytokine-cytokine receptor interaction
D
GO BP Down
-log10 adj. p-value
response to stimulus
response to chemical
multicellular organismal process
long-chain fatty acid transport
KEGG Down
-log10 adj. p-value
Regulation of lipolysis in adipocytes

FigS7